Published for SISSA by Springer

Received: *June 16, 2025*
Accepted: *December 15, 2025*
Published: *February 13, 2026*

Search for nonresonant new physics signals in high-mass dilepton events produced in association with b-tagged jets in proton-proton collisions at $\sqrt{s} = 13$ TeV

The CMS collaboration

E-mail: cms-publication-committee-chair@cern.ch

Abstract: A search for nonresonant new physics phenomena in high-mass dilepton events produced in association with b-tagged jets is performed using proton-proton collision data collected in 2016–2018 by the CMS experiment at the CERN LHC, at a center-of-mass energy of 13 TeV corresponding to an integrated luminosity of 138 fb^{-1}. The analysis considers two effective field theory models with dimension-six operators; involving four-fermion contact interactions between two leptons ($\ell\ell$, electrons or muons) and b or s quarks (bb$\ell\ell$ and bs$\ell\ell$). Two lepton flavor combinations (ee and $\mu\mu$) are required and events are classified as having 0, 1, or $\geq$2 b-tagged jets in the final state. No significant excess is observed over the standard model backgrounds. Upper limits are set on the production cross section of the new physics signals. These translate into lower limits on the energy scale Λ of 6.9 to 9.0 TeV in the bb$\ell\ell$ model, depending on model parameters, and on the ratio of energy scale and effective coupling, Λ/g_*, of 2.0 to 2.6 TeV in the bs$\ell\ell$ model. Lepton flavor universality is also tested by comparing the dielectron (ee) and dimuon ($\mu\mu$) mass spectra for different b-tagged jet multiplicities. No significant deviation from the standard model expectation of unity is observed.

Keywords: Beyond Standard Model, Hadron-Hadron Scattering, Lepton Production

ArXiv ePrint: 2506.13565

https://doi.org/10.1007/JHEP02(2026)141

Contents

JHEP02(2026)141

1 Introduction

The standard model (SM) of particle physics successfully describes the known fundamental particles and the interactions between them. However, it fails to answer many open questions in particle physics, such as the nature of dark matter, the matter-antimatter asymmetry in the universe, the hierarchy problem, and the nonzero mass of neutrinos. To address the incompleteness of the SM, many theories beyond the SM have been introduced that predict the existence of new physics (NP) at the multi-TeV scale; a number of experiments at the CERN LHC are actively engaged in searches for NP signatures.

Searches for the resonant or nonresonant production of new physics at high invariant masses of dilepton events have played a central role in these programs. No significant sign of NP has been observed in these searches so far, with the latest results from the CMS and ATLAS Collaborations using proton-proton (pp) collision data at a center-of-mass energy $\sqrt{s} = 13\,\text{TeV}$ collected during Run 2 of the LHC (2015–2018) [1–3]. Traditionally, these searches have mostly focused on final states inclusive in the number of b-tagged jets. Recently, the ATLAS Collaboration published a search for nonresonant dilepton production in association with a b-tagged jet using the Run 2 data [4], and the CMS Collaboration published a search for the resonant production of $\mu\mu$ pairs in association with b-tagged jets with a similar data set, corresponding to an integrated luminosity of $138\,\text{fb}^{-1}$ [5].

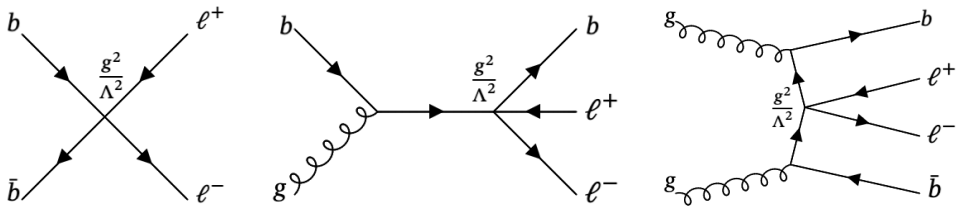

Figure 1. Representative Feynman diagrams for the production of dileptons via the bb$\ell\ell$ operator at the LHC, in association with 0 (left), 1 (center), and 2 (right) final state b quarks.

This paper presents the first search from CMS for new physics featuring the nonresonant production of dileptons in association with b-tagged jets using the pp collision data, collected from 2016 to 2018 and corresponding to an integrated luminosity of 138 fb^{-1}. This search specifically considers the interaction of the NP state with b quarks. The third-generation quark doublet is expected to be the most sensitive to NP because of the high mass of the quarks, and indeed hints of possible NP contributions have been given by experimental results on lepton flavor universality violation in B meson decays, notably in $R(\text{D}^0)$ and $R(\text{D}^*)$ [6].

The signal models considered in this analysis predict the nonresonant production of opposite-sign, same-flavor lepton pairs (e^+e^-, $\mu^+\mu^-$) in association with heavy-flavor jets. The nonresonant production of the NP can be modeled using effective field theory (EFT) techniques by integrating out the new degrees of freedom. Since the masses of the NP states associated with the signal are considered to be inaccessible at LHC energies, the models are described as a contact interaction (CI) between two leptons and two quarks ($\text{b}\bar{\text{b}}$ or $\text{b}\bar{\text{s}}$), resulting in a nonresonant excess of events at high mass. We target two such EFT models with dimension-six operators. One of the models is based on a pair of b quarks and a pair of charged leptons (bb$\ell\ell$ model), which can be generated by a tree-level exchange of a heavy neutral gauge boson Z′ [7] or scalar leptoquarks (LQs) [8–11]. Depending on how many of these b quarks are sea quarks from within the colliding protons, the dilepton system is produced in association with 0 to 2 b quarks in the final state. The analysis therefore targets different b-tagged jet multiplicities (0, 1, and $\geq$2 b-tagged jets). Figure 1 shows the representative Feynman diagrams for the production of lepton pairs via the bb$\ell\ell$ operator at the LHC, in association with 0 (left), 1 (center), and 2 (right) final state b quarks.

The other model probed in this analysis considers the flavor-changing neutral current (FCNC) $\text{b} \to \text{s}\ell^+\ell^-$ transition (bs$\ell\ell$ model), which is highly suppressed in the SM since it can only occur at loop level owing to the Glashow-Iliopoulos-Maiani (GIM) mechanism [12]. The $\text{b} \to \text{s}\ell^+\ell^-$ transition is expected to be mediated by a Z′ [13] or an LQ [14, 15], with flavor-violating couplings to b and s quarks, as well as couplings to either electrons or muons, as shown in figure 2. Any significant deviation from SM predictions in this channel would be a strong indication of beyond the SM physics. To target this model, ee and $\mu\mu$ channels with exactly 0 and 1 b-tagged jets are considered.

In addition to these two search strategies, lepton flavor universality is tested in these final states by measuring the $\mu\mu$-to-ee ratio for different b-tagged jet final states and comparing it to the corresponding SM expectation, after correcting for the differences in detector response,

JHEP02(2026)141

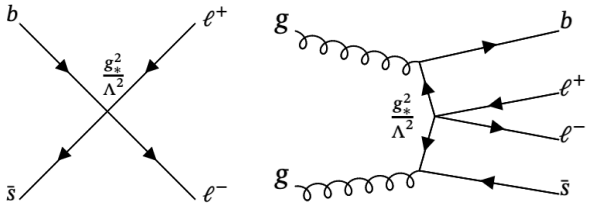

Figure 2. Representative Feynman diagrams for the production of dileptons via the bs$\ell\ell$ operator at the LHC, in association with 0 (left) and 1 (right) final state b quarks.

lepton acceptances, and lepton efficiencies. In contrast to the SM, the CI models predict a deviation from lepton universality [16], which would manifest itself in the $\mu\mu$-to-ee differential cross section ratios.

Tabulated results are provided in the HEPData record for this analysis [17].

2 The CMS detector

The central feature of the CMS apparatus is a superconducting solenoid of 6 m internal diameter, providing a magnetic field of 3.8 T parallel to the proton beam axis. Within the solenoid volume are a silicon pixel and strip tracker, a lead tungstate crystal electromagnetic calorimeter (ECAL), and a brass and scintillator hadron calorimeter, each composed of a barrel and two endcap sections. Forward calorimeters extend the pseudorapidity (η) coverage provided by the barrel and endcap detectors. Muons are measured in gas-ionization detectors embedded in the steel flux-return yoke outside the solenoid. Events of interest are selected using a two-tiered trigger system. The first level (L1), composed of custom hardware processors, uses information from the calorimeters and muon detectors to select events at a rate of around 100 kHz within a fixed latency of 4 μs [18]. The second level, known as the high-level trigger (HLT), consists of a farm of processors running a version of the full event reconstruction software optimized for fast processing, and reduces the event rate to a few kHz before data storage [19]. A more detailed description of the CMS detector, together with a definition of the coordinate system used and the relevant kinematic variables, can be found in refs. [20, 21].

3 Signal models

To probe new physics at the TeV scale, physics models based on EFT are considered that involve a four-fermion CI between a pair of leptons and a pair of quarks. This EFT approach involves dimension-six operators and limits the degrees of freedom related to heavy NP states by integrating them out. The introduction of CIs yields a modified SM Lagrangian with a series of higher-dimensional operators that are suppressed by inverse powers of the NP scale Λ:

$$\mathcal{L}_{\text{eff}} = \mathcal{L}_{\text{SM}} + \frac{1}{\Lambda^2}\mathcal{L}_2 + \ldots, \tag{3.1}$$

where $\mathcal{L}_{\text{SM}}$ is the usual SM Lagrangian. The analysis focuses on two signal models based on this EFT approach.

JHEP02(2026)141

In the bb$\ell\ell$ model, we consider the contribution of dimension-six operators to the $q\bar{q} \to \ell^+\ell^-$ process via a four-fermion CI between b quarks and a pair of opposite-sign, same flavor leptons (electrons and muons). The effective Lagrangian for the $b\bar{b}e^+e^-$ and $b\bar{b}\mu^+\mu^-$ interaction can be written as:

$$\mathcal{L}_{\text{eff}} = \mathcal{L}_{\text{SM}} + \frac{g^2}{\Lambda^2} \sum_{i,j=\text{L,R}} \eta_{ij} (\bar{b}_i \gamma_\mu b_i)(\bar{\ell}_j \gamma^\mu \ell_j), \tag{3.2}$$

where ℓ stands for e or μ and Λ is the scale of NP. The coupling strength g is assumed to be $\sqrt{4\pi}$, following the convention in ref. [7]. The four-fermion CI consists of four possible chirality structures described by the $\eta_{ij} = \pm 1$ term (left-handed quarks going to left-handed leptons (left-left, LL), left-handed quarks going to right-handed leptons (left-right, LR), etc.). By convention, only one of these possibilities is assumed to be realized in Nature at a time, setting the corresponding η_{ij} to 1 and all others to zero. The sign of the η_{ij} determines the sign of the interference of the signal with the SM Drell-Yan (DY) process, which can be either constructive ($\eta_{ij} = +1$) or destructive ($\eta_{ij} = -1$). This results in separate subclasses of this signal model, and all of them are considered in this analysis. It should be noted that the relative contribution from these CIs, compared to the SM DY process, grows with energy. For values of Λ comparable to or smaller than the highest dilepton mass recorded at the LHC, the EFT expansion would diverge and lose validity. In this analysis, the lower limits on Λ are set well above the maximum dilepton mass considered ($\approx 3.5\,\text{TeV}$), ensuring that the expansion safely converges in the probed parameter space [22].

The bs$\ell\ell$ model considers the $b \to s\ell^+\ell^-$ transition with flavor-violating coupling to b and s quarks as well as couplings to either electrons or muons. The model is described by the effective Lagrangian

$$\mathcal{L}_{\text{eff}} = \mathcal{L}_{\text{SM}} + \frac{C_{ij}^{U\ell}}{v^2} (\overline{u}_{\text{L}}^i \gamma_\mu u_{\text{L}}^j)(\bar{\ell}_{\text{L}} \gamma_\mu \ell_{\text{L}}) + \frac{C_{ij}^{D\ell}}{v^2} (\overline{d}_{\text{L}}^i \gamma_\mu d_{\text{L}}^j)(\bar{\ell}_{\text{L}} \gamma_\mu \ell_{\text{L}}), \tag{3.3}$$

where $\mathcal{L}_{\text{SM}}$ denotes the SM Lagrangian, whose FCNC contributions are highly suppressed. The additional terms describe the EFT operators mediating transitions of up-type and down-type quarks to a lepton pair, respectively, with v being the vacuum expectation value of the Higgs field. The flavor structure of the interaction is defined by the matrices $C_{ij}^{U\ell}$ and $C_{ij}^{D\ell}$, which are of the form:

$$C_{ij}^{U\ell} = \begin{pmatrix} C_{\text{u}\ell} & 0 & 0 \\ 0 & C_{\text{c}\ell} & 0 \\ 0 & 0 & C_{\text{t}\ell} \end{pmatrix}, C_{ij}^{D\ell} = \begin{pmatrix} C_{\text{d}\ell} & 0 & 0 \\ 0 & C_{\text{s}\ell} & C_{\text{bs}\ell}^* \\ 0 & C_{\text{bs}\ell} & C_{\text{b}\ell} \end{pmatrix}. \tag{3.4}$$

Here, the $C_{\text{bs}\ell}$ term defines the new physics component and is given by the effective coupling (g_*) and energy scale (Λ) via $C_{\text{bs}\ell} = g_*^2 v^2/\Lambda^2$, so that the ratio Λ/g_* is the free parameter of the model.

4 Event simulation

Simulated Monte Carlo (MC) samples are generated for both the SM backgrounds and the new physics signals. The SM DY+jets, WZ, ZZ, and VVV (V = W, Z) processes are

JHEP02(2026)141

simulated at next-to-leading order (NLO) in perturbative quantum chromodynamics using MadGraph5_aMC@NLO v2.6.5 [23]. The FxFx [24] scheme is used to match jets from matrix element calculations and parton showers. The DY+jets samples are produced binned in both the dilepton invariant mass ($m_{\ell\ell}$) and the number of additional jet emissions, with a sample size large enough to ensure sufficient events at high $m_{\ell\ell}$ in different b-tagged jets final states. The $\mathrm{t\bar{t}}$, tW, WW, and SM Higgs boson processes are simulated at NLO using the powheg 2.0 [25–31] event generator. The diboson processes, including WW, WZ, and ZZ, are referred to as VV processes.

Event samples for both EFT models considered in the analysis are generated with different values for Λ. Events are generated at leading order (LO) by interfacing the FeynRules UFO [7, 13, 32] model for $\mathrm{bb}\ell\ell$ ($\mathrm{bs}\ell\ell$) with MadGraph5_aMC@NLO v2.6.5 (v2.9.9). The MLM [33] scheme is used for jet matching. For the $\mathrm{bb}\ell\ell$ signal with constructive interference, samples are generated for Λ values between 6 and 26 TeV in steps of 4 TeV, split into four exclusive bins in the dilepton invariant mass with lower bin edges at 300, 800, 1300, and 2000 GeV. For destructive interference, the samples are simulated with both NP and SM DY contributions to ensure net positive cross sections in these samples. These samples are generated with Λ values between 4 and 18 TeV in steps of 2 TeV, split into four exclusive bins in the dilepton invariant mass with lower bin edges at 300, 800, 1300, and 2000 GeV. The samples are generated for all possible chirality structures (LL, LR, RL, RR) with $\eta_{ij} = \pm 1$, where the sign implies constructive (+1) or destructive (−1) interference with the SM DY process. For the $\mathrm{bs}\ell\ell$ model, samples are generated with Λ/g_* values ranging from 1 to 6 TeV in steps of 1 TeV, split into four exclusive bins in the dilepton invariant mass with lower bin edges at 200, 500, 1000, and 2000 GeV.

The event generator outputs are interfaced with pythia 8.230 [34] for parton showering and hadronization, using the CP5 (CP2) tune [35] for background (signal) samples. For all samples, the parton distribution functions (PDFs) are described with the NNPDF3.1 PDF set, computed at next-to-NLO [36] for background and LO for signal samples. The response of the CMS detector is simulated using the Geant4 [37] package.

All samples are normalized to the integrated luminosity using the cross section calculated by the respective event generator. The presence of multiple pp interactions in the same or adjacent bunch crossings (pileup) is incorporated by simulating additional interactions that are both in-time and out-of-time with the collision. The pileup in data is estimated based on the instantaneous luminosity measurements and the assumed inelastic pp cross section. The simulated samples are reweighted such that the pileup profile matches the one observed in data, based on measurements of the luminosity and assuming that the pp inelastic cross section is 69.2 mb [38].

Because of the limited time resolution of the different subdetectors, objects in the L1 trigger can be assigned to the wrong bunch crossing, which can lead to a loss of events ("trigger prefiring"). While normally negligible, a slowly increasing shift of the reconstructed cluster time in the ECAL occurred in the L1 trigger during the 2016 and 2017 data taking, predominantly at high $|\eta|$. The resulting efficiency loss is not included in simulation, and simulated events are reweighted to account for this inefficiency [39]. Similarly, a nonnegligible amount of trigger prefiring affected the L1 muon trigger during 2016 and to a lesser degree in 2017 and 2018, and this is taken into account in the analysis.

JHEP02(2026)141

5 Object reconstruction

The reconstruction and selection of leptons in this analysis are largely unchanged from previous searches for new physics at large $m_{\ell\ell}$ [1]. Compared to the previous results, the current analysis considers the b-tagged jets in the final state to target different signal models, and the data have been reprocessed to account for updated calibrations of the detector.

A full reconstruction of the events is performed using a particle-flow (PF) algorithm [40], which is based on an optimized combination of information from all subdetectors. The result is a list of PF candidates (electrons, muons, photons, as well as charged and neutral hadrons). The primary vertex is taken to be the vertex corresponding to the highest transverse momentum (p_{T}) scattering in the event, evaluated using tracking information alone, as described in section 9.4.1 of ref. [21].

To be selected in the L1 trigger, events in the ee channel must contain at least two electron candidates passing certain p_{T} thresholds. The thresholds evolved with time but never exceeded 25 (17) GeV for the higher-(lower-)p_{T} electron. To protect against possible inefficiencies of the L1 trigger for electrons, events containing at least one electron, jet, or tau candidate passing significantly higher p_{T} thresholds at L1 are also included at the HLT level. In the HLT, the presence of two electrons with $p_{\mathrm{T}} > 33$ (25) GeV was required in 2016 and 2017 (2018).

Electron candidates are reconstructed from energy clusters in the ECAL, which are combined with matching tracks in the tracking system [41]. The ECAL clustering groups together energy deposits that are compatible with having originated from the same particle, thus recovering energy losses due to bremsstrahlung. The angular information of the electron candidate is derived by combining information from the ECAL cluster and the associated track.

Electron candidates with $p_{\mathrm{T}} > 35$ GeV and $|\eta_C| < 1.44$ (ECAL barrel region) or $1.57 < |\eta_C| < 2.50$ (ECAL endcap region) are selected, where η_C is the pseudorapidity of the electron's ECAL cluster. As the quality of ECAL cluster reconstruction is lower in the transition region $1.44 < |\eta_C| < 1.57$, electrons falling in that range are rejected. The electron candidates are required to pass selection and isolation criteria optimized for highly energetic electrons [41], which include a transverse impact parameter requirement of $|d_{\mathrm{xy}}| < 0.02$ cm in the barrel and $|d_{\mathrm{xy}}| < 0.05$ cm in the endcap, relative to the primary vertex. These criteria suppress backgrounds from pions, photon conversions, and electrons in jets. The electron efficiency scale factor (SF) is close to unity for both barrel and endcap, with an uncertainty ranging from 1–3% across the p_{T} range of 35–1000 GeV, and set to 3% above 1000 GeV.

The efficiency to trigger on, reconstruct, and identify high-p_{T} electrons has been studied in detail using $\mathrm{Z} \to \mathrm{ee}$ candidate events and has been validated in data up to p_{T} values of 1 TeV. In the analysis, simulated events are not required to pass the trigger selection, instead are weighted by the trigger efficiency measured in data. The trigger efficiency is observed to be >95% for all data-taking years.

In the L1 trigger, events containing a single muon with $p_{\mathrm{T}} > 22$ GeV are accepted. At the HLT, this threshold is 50 GeV throughout the whole data-taking period, while additional triggers using complementary reconstruction algorithms and a p_{T} threshold of 100 GeV were added in 2017 and 2018 to maximize efficiency for high-p_{T} muons. Muons within $|\eta| < 2.4$ are accepted [42].

JHEP02(2026)141

Muons are reconstructed by combining the hits in the tracker and muon chambers. For muons with $p_T > 200\,\text{GeV}$, the TuneP algorithm is used to take into account radiative energy losses in the detector material [43]. Muons are required to have $p_T > 53\,\text{GeV}$ and $|\eta| < 2.4$. A set of selection criteria is applied that is optimized for high-p_T muons [43]. Muons produced inside jets are rejected by requiring that the scalar sum of the p_T of all tracks not belonging to the muon candidate in a cone of $\Delta R = \sqrt{(\Delta\eta)^2 + (\Delta\phi)^2} < 0.3$ around the muon does not exceed 5% of the muon's p_T. To further improve the selection purity of prompt muons, the muon track is required to have longitudinal distance $|d_z| < 0.1\,\text{cm}$, and transverse distance $|d_{xy}| < 0.02\,\text{cm}$ with respect to the primary vertex.

The efficiency of muons to pass the trigger, identification, and isolation requirements has been measured using $Z \to \mu\mu$ candidate events and validated up to 1 TeV. The efficiencies are stable as a function of p_T, with the exception of a slight loss of trigger efficiency at high p_T, caused by muons showering in the detector material and failing the L1 trigger. The SFs are observed to be close to unity, and are applied to the simulated events to account for small differences in efficiencies observed between data and simulation.

Using high-p_T muons originating from Lorentz-boosted Z bosons, the description of the muon momentum resolution in simulation has been compared with the data. Although good agreement is observed for central muons, the simulation underestimates the resolution effects for forward muons with $|\eta| > 1.2$ by $\approx 15\%$. The p_T values of these muons in simulated events have been smeared to account for this difference.

Jets are reconstructed from all PF candidates using the anti-k_T clustering algorithm [44, 45] with a distance parameter of 0.4. Identification criteria are applied to jet candidates to remove anomalous effects from the calorimeters [38]. For jets with $p_T > 20\,\text{GeV}$, the identification efficiency is >90% depending on η. Jet energy scale (JES) corrections are applied to the measured jet energy depositions to correct for any offset due to energy coming from pileup interactions, miscalibration of the detector response to hadrons, and the residual differences between data and simulation as a function of the jet p_T and η. Jets are required to have $p_T > 20\,\text{GeV}$ and $|\eta| < 2.4$. Jets originating from the hadronization of b quarks are identified using the DeepJet algorithm [46, 47]. The b quark jet with the highest p_T is required to satisfy the tight identification criteria, for which the identification efficiency is approximately 50% (depending on p_T, η, and data-taking year), and the misidentification rate for light-flavor quark or gluon jets is 0.1% and for c quark jets is 2.4%. The other b quark jets in the event are required to satisfy relaxed requirements, for which the typical efficiency is 68% (depending on p_T, η, and data-taking year), and the misidentification rate for light-flavor quark or gluon jets is 1.0% and for c quark jets is 12%. The choice of tight and relaxed working points is made following the dedicated optimization studies within the CMS b tagging framework, thus maximizing the overall signal significance across the different b-tagged jet final states. The SFs are applied to correct for the difference in b tagging performance between data and simulation [48].

The missing transverse momentum $\vec{p}_T^{\,\text{miss}}$ is the negative vector p_T sum of all PF candidates [49]. Its magnitude is p_T^{miss}. The JES corrections are propagated to p_T^{miss}, which improves agreement in p_T^{miss} between simulation and data. Since the PF algorithm does not consider the dedicated high-p_T muon reconstruction using the TuneP algorithm, the $\vec{p}_T^{\,\text{miss}}$ is also corrected for the difference in muon p_T between the PF and TuneP algorithms.

JHEP02(2026)141

6 Event selection

To search for a nonresonant excess of events in the dilepton mass spectra, electron or muon pairs are selected, where the leptons pass the selection described in the previous section. Since the charge misidentification probability increases significantly with electron p_{T}, resulting in a significant efficiency loss from an opposite-sign selection, no charge requirement is made for electron pairs. The fraction of same-sign events in DY simulation increases from about 1% at the Z boson peak to $\approx 10\%$ for ee masses of several TeV. In data, it is consistent with this expectation [1, 41]. In the case of muon pairs, the charge misidentification probability is of the order of 10^{-4} for high-p_{T} ($\approx 2\,\mathrm{TeV}$) muons [43]. Therefore, the two muons are required to have opposite electric charge. To suppress the contribution of muons resulting from cosmic rays, the angle between the two muons is required to be less than $\pi - 0.02$. In the $\mu\mu$ channel, any event with an electron passing loose selection requirements with $p_{\mathrm{T}} > 10\,\mathrm{GeV}$ and $|\eta| < 2.5$ is rejected, and in the electron channel events with a muon passing loose selection requirements with $p_{\mathrm{T}} > 10\,\mathrm{GeV}$ and $|\eta| < 2.4$ are rejected.

For events containing more than two electrons or two muons (<1%), originating mostly from WZ and ZZ production, the pair with an invariant mass $m_{\ell\ell}$ closest to the Z boson mass is considered. If no pair is found within 20 GeV of the nominal Z boson mass, the pair with the highest-p_{T} leptons is retained [50]. Finally, the search for NP is performed in events with $m_{\ell\ell} > 200$ (300) GeV for the bs$\ell\ell$ (bb$\ell\ell$) signal and the events with $120 < m_{\ell\ell} < 200\,\mathrm{GeV}$ are selected for a control region (CR) to estimate the DY+jets contribution.

In both the ee and $\mu\mu$ channels, the events are divided into two categories based on the lepton $|\eta|$ [1]. This increases the sensitivity of the analysis by including the differences in lepton reconstruction performance and background levels between the central and forward parts of the detector. The "barrel-barrel" (BB) category is defined as both leptons having $|\eta| < 1.44\,(1.20)$ for electrons (muons). The "barrel-endcap" (BE) category contains events where at least one electron (muon) has $|\eta| > 1.56\,(1.20)$. Events with both leptons in the endcap (EE) are included in the BE category in the $\mu\mu$ channel, whereas such events in the ee channel are rejected owing to a higher contribution of background in this channel. The events are then sorted into final state categories for zero b-tagged jets ("0b"), exactly one b-tagged jet ("1b"), and two or more b-tagged jets ("2b"). The $m_{\ell\ell}$ distributions are further divided into analysis bins according to the b-tagged jet final states. Since the signal sensitivity depends on the binning, a dedicated study is performed to establish the optimal choice. For the 0b and 1b final states, the lower bin edges are set at 200, 300, 400, 500, 700, 1100, and 1900 GeV, with an overflow bin above 1900 GeV. For the 2b final state, the lower bin edges are set at 200, 400, 600, and 900 GeV, with an overflow bin above 900 GeV. For the bb$\ell\ell$ signal, the binning is the same as for the bs$\ell\ell$ signal, except that the first bin starts at 300 GeV instead of 200 GeV.

In the 1b and 2b final states, the dominant source of SM background arises from $\mathrm{t\bar{t}}$ production. To suppress this background, a deep neural network (DNN) based selection is used. The network is implemented using the PyTorch framework and trained separately for the ee and $\mu\mu$ channels, and for each data-taking year, using variables where signal and background show significant differences, such as lepton and b-tagged jet kinematic distributions, $p_{\mathrm{T}}^{\mathrm{miss}}$, the minimum invariant mass of a lepton and a b-tagged jet, and the minimum 3D angle between

JHEP02(2026)141

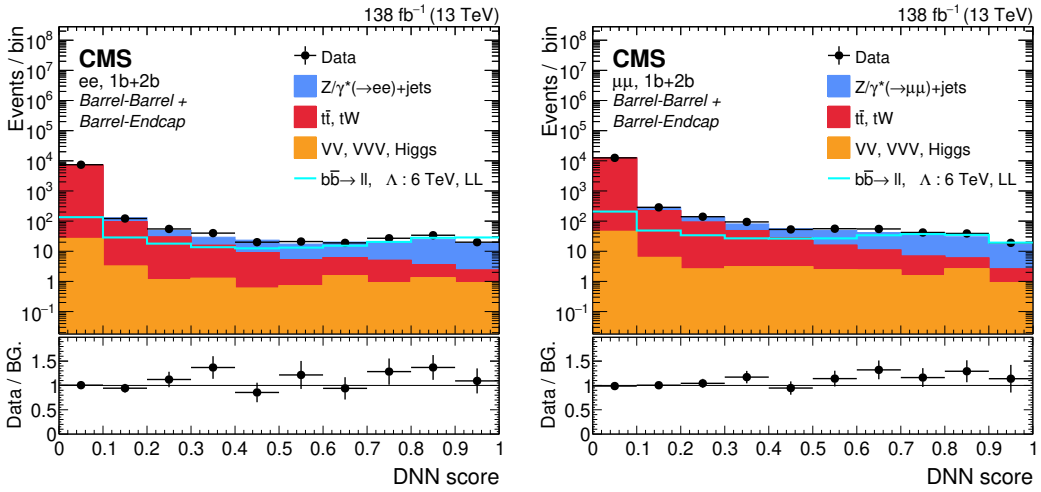

Figure 3. Observed data and various SM backgrounds in bins of DNN score evaluated from per-year and per-pseudorapidity trained models in the ee (left) and $\mu\mu$ (right) channels. The solid cyan line in the upper panels correspond to the bb$\ell\ell$ signal expectation for $\Lambda = 6$ TeV in the LL constructive interference model. The lower panel of each plot shows the ratio of data to predicted background yields.

the leading lepton and a b-tagged jet. The network is trained using one representative bb$\ell\ell$ signal sample ($\Lambda = 6$ TeV), and it was verified that the discriminating power does not degrade when it is applied to other signal models.

The network is trained using the binary cross entropy loss classifier function, which measures the dissimilarity between true labels ($y_i = 1$ for signal and $y_i = 0$ for background) and the predicted probabilities for signal classification, optimizing the network to classify signal and background events effectively. For training the network, 80% of this representative MC sample is selected, with the remaining 20% used for validating the trained network. In addition, the final evaluation of the trained model is performed on independent data sets, drawn from different MC samples that are not used in training or validation, ensuring an unbiased performance assessment. The network is set to have four hidden layers with 128, 64, 32, and 16 nodes, respectively. The learning rate is varied at each epoch using an exponential decay scheduler and gradually decreases. The training is performed in 20 epochs, where it reaches the minimum and flat validation loss. This helps the model converge more effectively and provides a good balance between fast initial convergence and fine-tuning as the training progresses. Training and validation losses are found to be consistent, and the DNN score distributions for the training, validation, and testing data sets are in good agreement, confirming that overfitting is negligible. Figure 3 shows the DNN score, after combining models trained per-year, for data and SM backgrounds in the ee (left) and $\mu\mu$ (right) channels. The plots are shown after applying the full signal region (SR) selections but before applying any scale factor corrections to the simulated $\mathrm{t\bar{t}}$ and DY+jets events. The contribution from nonprompt leptons is not shown, since it is negligible in the $\mu\mu$ channel and below 1% in the ee channel. The DNN score is required to be greater than 0.6 as this gives the best signal significance in simulation. Upon selecting events with this DNN score

JHEP02(2026)141

	$m_{\ell\ell}$ range	Lepton flavor	DNN score	N_{b}
0b bs$\ell\ell$ (bb$\ell\ell$) SR	>200 (300) GeV	ee, $\mu\mu$	—	=0
1b bs$\ell\ell$ (bb$\ell\ell$) SR	>200 (300) GeV	ee, $\mu\mu$	>0.6	=1
2b bs$\ell\ell$ (bb$\ell\ell$) SR	>200 (300) GeV	ee, $\mu\mu$	>0.6	≥2
DY CR	120–200 GeV	ee, $\mu\mu$	—	≥0
$\mathrm{t\bar{t}}$ CR	>200 GeV	eμ	—	≥0
$\mathrm{t\bar{t}}$ VR	>200 GeV	eμ	>0.6	≥1

Table 1. Definitions of the SRs, CRs and VRs.

in the 1b and 2b final states, 90% of $\mathrm{t\bar{t}}$ events are rejected; the DY+jets process becomes the dominant background in all event categories in the SR.

7 Background estimation

Background processes producing electrons and muons are estimated from simulation. Dedicated control regions (CRs) are used to derive SFs that correct for possible mismodeling in simulation. The simulation of the dominant DY+jets background is corrected by comparing the simulated $m_{\ell\ell}$ spectra with those observed in data in the DY+jets CR, separately for ee and $\mu\mu$ events. Before making this comparison, the $\mathrm{t\bar{t}}$ MC sample is corrected for any mismodeling of the selection efficiencies in simulation with an SF derived in the $\mathrm{t\bar{t}}$ CR ($\mathrm{SF_{t\bar{t}}}$) as a function of the number of b jets, N_{b}, as described below. For the $\mathrm{t\bar{t}}$ process, additional validation regions (VRs) are used to verify the accuracy of these SFs before applying them in the SRs. The SR, CR and VR definitions are summarized in table 1.

The $\mathrm{t\bar{t}}$ CR is obtained by selecting an oppositely charged, different-flavor lepton pair (eμ), where all the selection criteria for the e and μ are kept the same as to those in the SR with $m_{\ell\ell} > 200\,\mathrm{GeV}$, except no DNN score selection is applied in this region. The resulting $\mathrm{SF_{t\bar{t}}}$ is given by:

$$\mathrm{SF_{t\bar{t}}} = (N_{\mathrm{e}\mu}^{\mathrm{Data}} - N_{\mathrm{e}\mu}^{\text{non-t}\bar{\text{t}}\ \ \mathrm{MC}})/N_{\mathrm{e}\mu}^{\mathrm{t\bar{t}\,MC}}. \tag{7.1}$$

Here $N_{\mathrm{e}\mu}^{\mathrm{Data}}$ are the events observed in the $\mathrm{t\bar{t}}$ CR in data, and $N_{\mathrm{e}\mu}^{\text{non-t}\bar{\text{t}}\ \ \mathrm{MC}}$ and $N_{\mathrm{e}\mu}^{\mathrm{t\bar{t}\,MC}}$ are the events observed in the $\mathrm{t\bar{t}}$ CR in non-$\mathrm{t\bar{t}}$ MC samples and $\mathrm{t\bar{t}}$ MC samples, respectively. Because of the low event count in the $N_{\mathrm{b}} > 3$ category, the $\mathrm{SF_{t\bar{t}}}$ estimated from the $N_{\mathrm{b}} = 3$ bin is used for the higher N_{b} bins. The validation of simulation with data in the $\mathrm{t\bar{t}}$ CR is shown in figure 4 as a function of $m_{\mathrm{e}\mu}$ for the 0b (upper) and ≥1b (lower) channels. The purity of $\mathrm{t\bar{t}}$ events in the 0b channel is around 80%, whereas in the 1b and 2b channels, the purity is greater than 99%.

The values of $\mathrm{SF_{t\bar{t}}}$ measured in different bins of b jet multiplicity are listed in table 2 (3) for the BB (BE) category. The associated systematic uncertainties in the $\mathrm{SF_{t\bar{t}}}$ are determined by propagating the statistical uncertainties in the data and simulation yields.

Once the $\mathrm{t\bar{t}}$ events are corrected with this $\mathrm{SF_{t\bar{t}}}$, a validation of observed $\mathrm{t\bar{t}}$ events in simulation is performed after the DNN score selection in the 1b and 2b channels. The $\mathrm{t\bar{t}}$ validation region (VR) is a subset of $\mathrm{t\bar{t}}$ CR with the additional requirements of DNN score to be greater than 0.6 and ≥1 b-tagged jets. Figure 5 shows the comparison of data and various

JHEP02(2026)141

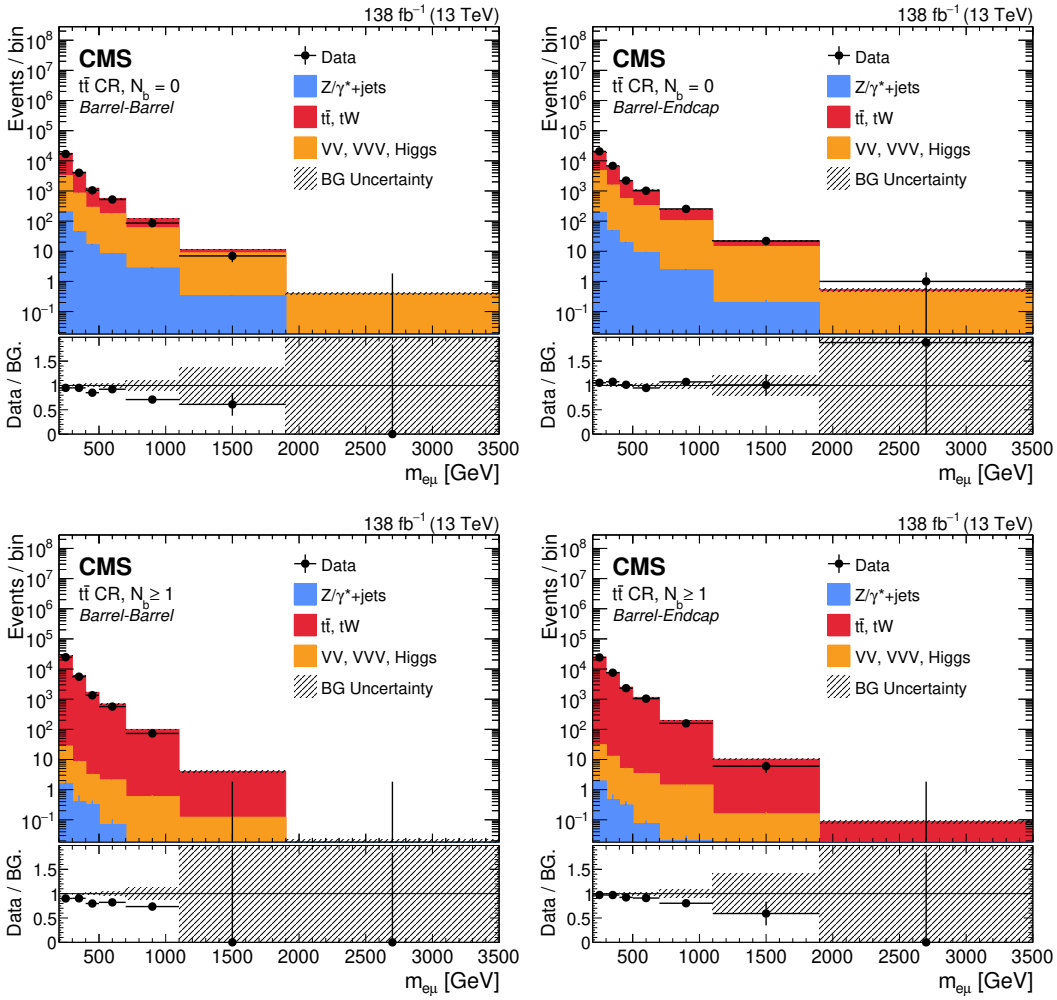

Figure 4. Comparison of data and various SM backgrounds in the $t\bar{t}$ CR as a function of $m_{e\mu}$ for the 0b (upper) and $\geq$ 1b (lower) channels in the BB (left) and BE (right) categories. The lower panel of each plot shows the ratio of data to predicted background yields before correction with $SF_{t\bar{t}}$ values. The hatched band in the lower panels indicates the statistical uncertainty in the simulated background prediction.

N_b	2016	2017	2018
0	0.92 ± 0.02	0.83 ± 0.01	0.84 ± 0.01
1	0.83 ± 0.01	0.83 ± 0.01	0.85 ± 0.01
2	0.84 ± 0.01	0.81 ± 0.01	0.83 ± 0.01
3	1.37 ± 0.10	1.15 ± 0.08	1.38 ± 0.07

Table 2. Measured values of the $SF_{t\bar{t}}$ in the OS $t\bar{t}$ CR (BB category).

SM processes in the $t\bar{t}$ VR after correcting with $SF_{t\bar{t}}$ values. The deviations from unity are taken to be the systematic uncertainty in the $t\bar{t}$ estimation in the SR.

Additionally, the shapes of simulated $t\bar{t}$ dilepton mass distributions as a function of $m_{e\mu}$ in the $t\bar{t}$ VR and m_{ee} ($m_{\mu\mu}$) in the SR are compared to ensure the robustness of the $t\bar{t}$

JHEP02(2026)141

N_b	2016	2017	2018
0	1.10 ± 0.02	1.04 ± 0.01	1.00 ± 0.01
1	0.93 ± 0.01	0.93 ± 0.01	0.95 ± 0.01
2	0.94 ± 0.02	0.88 ± 0.01	0.91 ± 0.01
3	1.54 ± 0.11	1.26 ± 0.08	1.40 ± 0.07

Table 3. Measured values of the $SF_{t\bar{t}}$ in the OS $t\bar{t}$ CR (BE category).

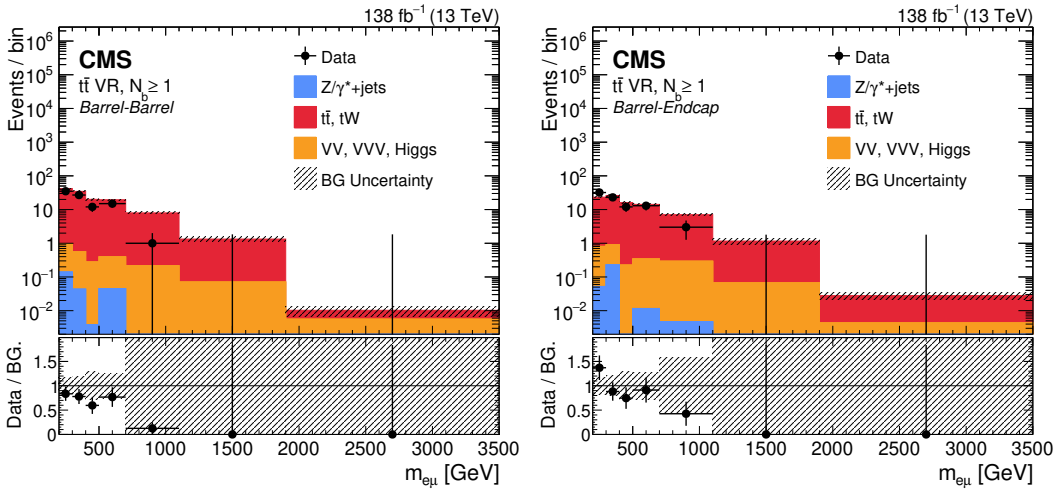

Figure 5. Comparison of data and various SM backgrounds in the $t\bar{t}$ VR as a function of $m_{e\mu}$ for the BB (left) and BE (right) categories. The lower panel of each plot shows the ratio of data to predicted background yields. The hatched band in the lower panels indicates the statistical uncertainty in the simulated background prediction.

modeling in the SR after the $SF_{t\bar{t}}$s are applied. The bin-by-bin deviations from unity in the ratio of the two distributions are considered as an additional systematic uncertainty, applied as a function of m_{ee} ($m_{\mu\mu}$) bins, in the $t\bar{t}$ background estimate in the SR. Figure 6 shows the ratio ($R_{e\mu/ee}$) of $m_{e\mu}$ and m_{ee} distribution for the BB (left) and BE (right) categories. Similarly, figure 7 shows the ratio ($R_{e\mu/\mu\mu}$) of $m_{e\mu}$ and $m_{\mu\mu}$ distribution for the BB (left) and BE (right) categories.

After correcting the $t\bar{t}$ MC sample, the residual differences observed in the DY+jets CR represent the mismodeling of the DY+jets MC sample. Similar to the $t\bar{t}$ CR, the SF_{DY} from the DY+jets CR are obtained as a function of N_b. These SF_{DY}s are measured as a difference between data and all SM processes in the DY+jets CR. Figure 8 shows the comparison between data and all SM processes in the DY+jets CR as a function of N_b in the ee (left) and $\mu\mu$ (right) channels. The data-to-simulation SF_{DY}s are derived separately for BB and BE categories for each data-taking year. In both the ee and $\mu\mu$ channels, the SF_{DY}s show a slight dependence on N_b, with values generally close to unity, indicating reasonable agreement between data and simulation. The SF_{DY}s in the 0b final state range from 0.92 to 0.96, while slightly higher variations are observed in the 1b and 2b final states, where the SF_{DY}s range from 0.92 to 1.10. The SF_{DY}s in the ee and $\mu\mu$ channels are consistent,

JHEP02(2026)141

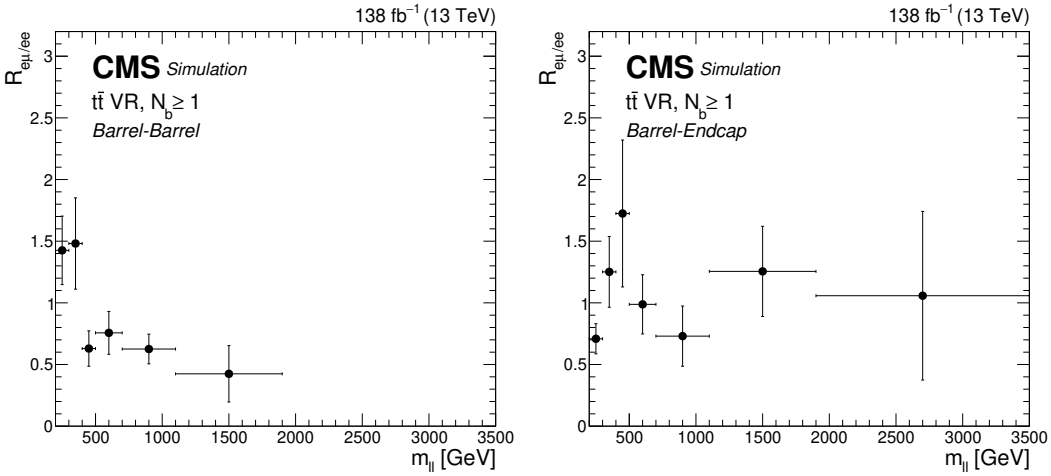

Figure 6. Ratio of simulated $t\bar{t} \to e\mu$ events with SR selections and simulated $t\bar{t} \to ee$ events in the SR for the BB (left) and BE (right) categories. The error bars represent the statistical uncertainty in the simulated event yields.

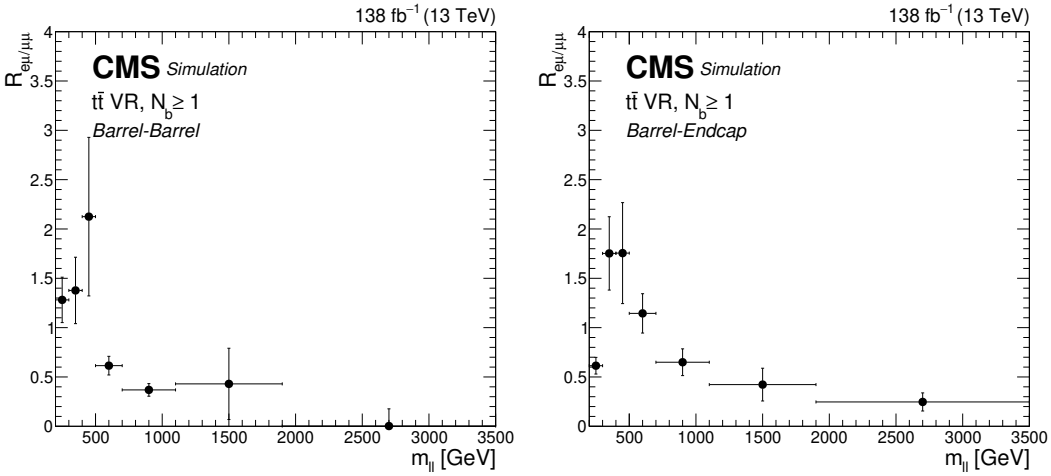

Figure 7. Ratio of simulated $t\bar{t} \to e\mu$ events with SR selections and simulated $t\bar{t} \to \mu\mu$ events in the SR for the BB (left) and BE (right) categories. The error bars represent the statistical uncertainty in the simulated event yields.

showing no significant discrepancies between the two CRs. All the simulated backgrounds are corrected with the observed SF_{DY}, and the associated statistical uncertainty in the SF_{DY} is taken to be the systematic uncertainty. An additional 10% uncertainty in the SF_{DY} is included in the systematic uncertainty for DY+jets background in the 1b and 2b final states to cover the deviations of data from prediction, and to take into account any bias because of the low number of events for the DY+jets process in these categories.

Background sources with nonprompt leptons and jets misidentified as leptons make very small contributions (1–3%), to both the ee and $\mu\mu$ channels. These backgrounds, jointly represented as "Jets" background in the following, are estimated using data CRs enriched

JHEP02(2026)141

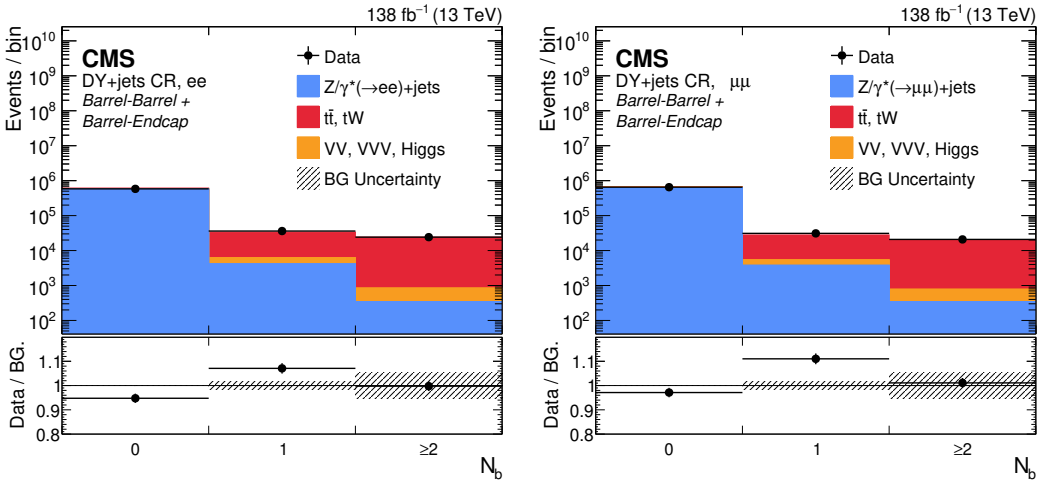

Figure 8. Comparison between data and various SM processes in DY+jets CR as a function of the number of b jets in the ee (left) and $\mu\mu$ (right) channels. The lower panel of each plot shows the ratio of data to predicted background yields. The hatched band in the lower panels indicates both the statistical and systematic uncertainty in the simulated background prediction.

in multijet events [51] by loosening the lepton identification requirements, in bins of p_T and η separately for the barrel and endcap regions. The fake rate is then applied to events in the SR where one or both leptons fail the tight identification but pass the preselection, after subtracting other background contributions estimated from simulation and correcting for double counting in dijet events. The method is validated in same-sign dilepton CRs for both the ee and $\mu\mu$ channels. To account for possible mismodeling of fake contributions, a conservative 50% systematic uncertainty is assigned to the "Jets" background estimate. Even though the uncertainty in these estimates is high, these backgrounds have a negligible effect on the results owing to their small contribution.

8 Systematic uncertainties

The main experimental systematic uncertainties considered in this analysis include the uncertainty in the integrated luminosity, the modeling of pileup interactions, the lepton reconstruction, identification, and trigger efficiencies, as well as the energy scale and resolution of jets and the b tagging efficiencies. Additional uncertainties affecting the background estimates, such as scale factors derived in CRs, are also included.

The systematic uncertainty in the integrated luminosity measurement is 1.2% for 2016 data, 2.3% for 2017 data, and 2.5% for 2018 data, with an uncertainty of 1.6% for the combined sum of the three years [52–54]. Since the dominant background processes are normalized in data CRs, this uncertainty mainly affects the signal simulation. Systematic uncertainties related to the pileup reweighting were assessed by recalculating the weights, with the assumed value of the total inelastic cross section shifted up and down by 4.6% with respect to the nominal value [55]. The effect of this uncertainty is very small on signal and background (<1%).

JHEP02(2026)141

The effect of the JES uncertainty on the estimated event yields is $\approx 2\%$ for signal and background in the 1b final state and is around 2–4% in the 2b final state, whereas the effect of jet energy resolution (JER) uncertainty is negligible compared to the statistical uncertainty of the simulation. Uncertainties in the b tagging efficiency are estimated by varying the associated SFs by one standard deviation (SD) and computing the impact on the estimated event yields for background and signal. The SF depends on the flavor of the parton that originated the jet and the uncertainties are estimated for heavy-flavor (b and c) jets and light-flavor quark or gluon jets separately. The effect of this uncertainty is less than 5% for both signal and background.

Systematic effects due to imprecise knowledge of the PDFs in the SR are determined by reweighting the simulated mass distributions according to the replicas of the NNPDF3.1 next-to-NLO PDF set and computing the 68% interval of the observed changes, using the PDF4LHC prescription [56]. In addition to the PDF variations, uncertainties from variations of the renormalization and factorization scales are also evaluated by varying the scales by factors of 0.5 and 2.0, respectively. The contribution of the PDF and scale uncertainties at low mass ($<$1500 GeV) is $\approx 2\%$ and at high mass is $\approx 5\%$ for the DY+jets simulation. The uncertainty is significant for the subdominant $\mathrm{t\bar{t}}$ background, since it is initiated predominantly by gluon fusion, resulting in an uncertainty of around 30% at high mass. The combined PDF and scale uncertainty for signal samples is around 2% at high masses.

The overall event selection efficiency including trigger, reconstruction, identification, and isolation is assigned a relative uncertainty of 6 (8)% for barrel-barrel (barrel-endcap) events in the ee channel, whereas an uncertainty of 1–2% is assigned everywhere in the $\mu\mu$ channel.

The uncertainty in the electron energy scale is 2% in the barrel and 1% for the endcap region for all three years of data taking. The uncertainty in the ee mass resolution is negligible.

Potential biases in the muon momentum scale, particularly at high p_{T}, have been studied using the generalized endpoint method [43]. No bias has been found within the statistical uncertainties in the method. These uncertainties are hence assigned as systematic uncertainties in the muon p_{T} scale. The impact of this uncertainty is 1–2% for background events at high mass (3000–4000 GeV); whereas it is as large as 5% for signal events.

The uncertainty in the trigger prefiring rate in the forward region of the ECAL endcap in 2016 and 2017 is 20%, resulting in a 2–3% uncertainty in the acceptance for ee events. The effect of trigger prefiring rate on the acceptance of $\mu\mu$ events is less than 1%.

The statistical uncertainties associated with the SFs measured in DY+jets and $\mathrm{t\bar{t}}$ CRs are assigned as systematic uncertainties to the corresponding background estimates in the SR and are less than 1% in all cases. Additionally, the systematic uncertainty in the $\mathrm{t\bar{t}}$ estimation is derived from the deviations observed in the $\mathrm{t\bar{t}}$ VR in data and simulation after applying the DNN selection. Moreover, the systematic uncertainty based on shape differences between the $\mathrm{t\bar{t}}$ VR and SR is also considered. These uncertainties are applied in bins of dilepton invariant mass and range from 10–40%.

The systematic uncertainties in the highest two mass bins of dilepton mass distribution for DY+jets background are shown in table 4 (5) for the ee ($\mu\mu$) channels, respectively.

JHEP02(2026)141

	1100–1900 GeV	>1900 GeV
DY+jets normalization	1–10%	1–10%
Electron trigger	3.2%	3.2%
Electron identification and isolation	3.7%	3.7%
Electron energy scale	8.4%	11.5%
L1 prefiring	<0.1%	<0.1%
Pileup	0.4%	0.2%
PDF	2.8%	4.7%
JES	2.0%	2.0%
JER	0.5%	0.5%
b tagging heavy-flavor SF	3.0%	4.0%
b tagging light-flavor/gluon SF	2.8%	2.9%

Table 4. Systematic uncertainties for the DY+jets background prediction in the highest two mass bins for the ee channel. The values shown are post-fit, with all background scale factors applied. The uncertainties are evaluated inclusively across the b jet multiplicity and $|\eta|$ regions. The dominant sources of uncertainty remain consistent across the different categories.

	1100–1900 GeV	>1900 GeV
DY+jets normalization	1–10%	1–10%
Muon trigger	1.6%	2.0%
Muon reconstruction	0.8%	1.0%
Muon identification	0.7%	0.9%
Muon isolation	0.7%	0.9%
Muon mass scale	4.8%	5.5%
Muon resolution	0.1%	0.4%
L1 prefiring	0.1%	0.1%
Pileup	0.2%	0.1%
PDF	2.8%	4.7%
JES	2.0%	2.0%
JER	0.5%	0.5%
b tagging heavy-flavor SF	3.0%	4.0%
b tagging light-flavor/gluon SF	2.8%	2.9%

Table 5. Systematic uncertainties for the DY+jets background prediction in the highest two mass bins for the $\mu\mu$ channel. The values shown are post-fit, with all background scale factors applied. The uncertainties are evaluated inclusively across the b jet multiplicity and $|\eta|$ regions. The dominant sources of uncertainty remain consistent across the different categories.

9 Results

The invariant mass distributions in the ee and $\mu\mu$ channels in the 0b, 1b, and 2b final states are shown in figures 9–11, respectively. For illustration, the invariant mass distributions are overlaid for bb$\ell\ell$ signals with $\Lambda = 6$ and 18 TeV, with the LL chirality configuration and constructive interference. To obtain the background predictions shown in these figures, a

JHEP02(2026)141

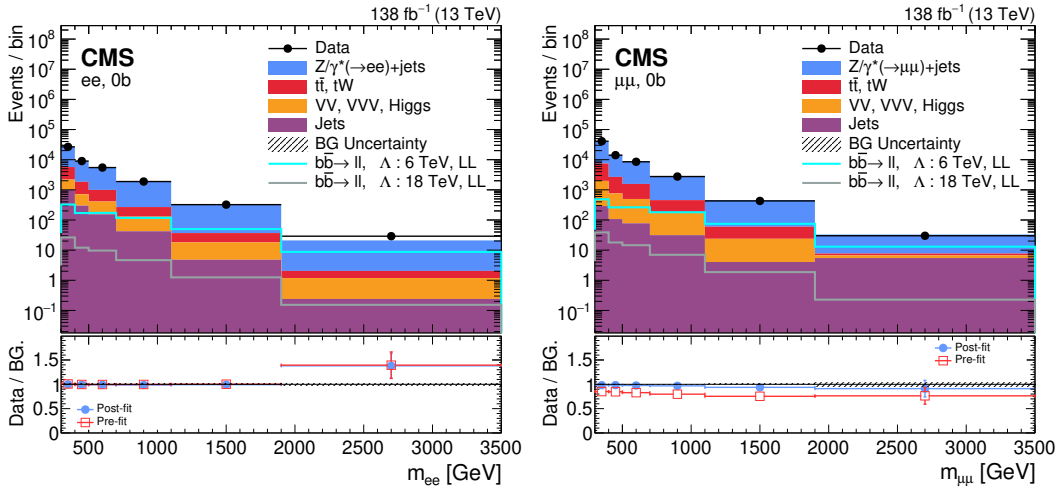

Figure 9. Observed $m_{\ell\ell}$ distributions in the data, and the post-fit backgrounds (stacked histograms), in the SR for ee+0b (left) and $\mu\mu$+0b (right) channels. The lower panels show ratios of the data to the pre-fit background prediction and post-fit background yield as red open squares and blue points, respectively. The hatched band in the lower panels indicates the systematic component of the post-fit uncertainty. The solid lines in the upper panels correspond to the bb$\ell\ell$ signal expectations, for $\Lambda = 6$ and 18 TeV in the LL constructive interference model.

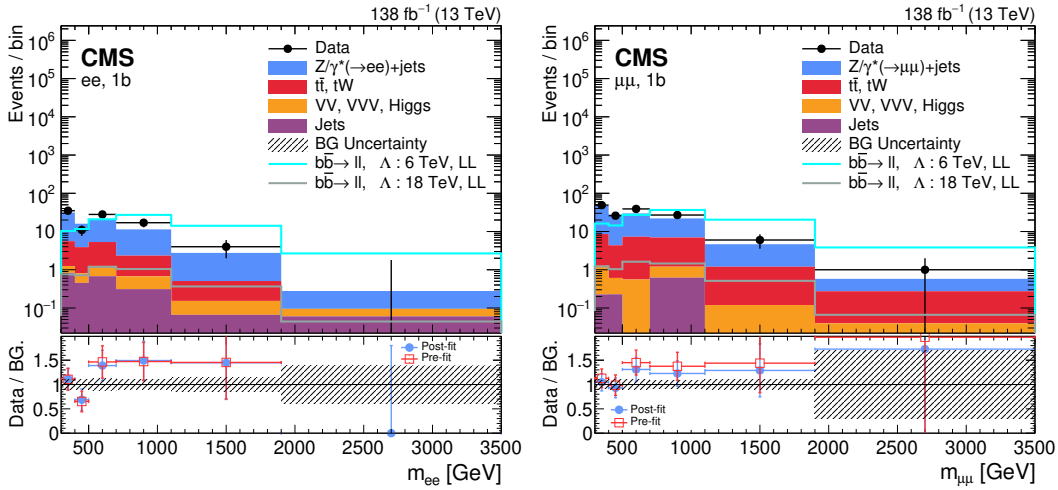

Figure 10. Observed $m_{\ell\ell}$ distributions in the data, and the post-fit backgrounds (stacked histograms), in the SR for ee+1b (left) and $\mu\mu$+1b (right) channels. The lower panels show ratios of the data to the pre-fit background prediction and post-fit background yield as red open squares and blue points, respectively. The hatched band in the lower panels indicates the systematic component of the post-fit uncertainty. The solid lines in the upper panels correspond to the bb$\ell\ell$ signal expectations, for $\Lambda = 6$ and 18 TeV in the LL constructive interference model.

simultaneous background-only maximum-likelihood fit is performed across all SRs, separated by b-tagged jet multiplicity and lepton η categories. The parameter of interest is the background normalization, with signal strength fixed to zero. The observed mass spectra shown in the plots are consistent with the SM predictions. A slight excess, with a significance of less than 2 SD, is seen in the ee channel for masses above 1.9 TeV (figure 9 left). This is

JHEP02(2026)141

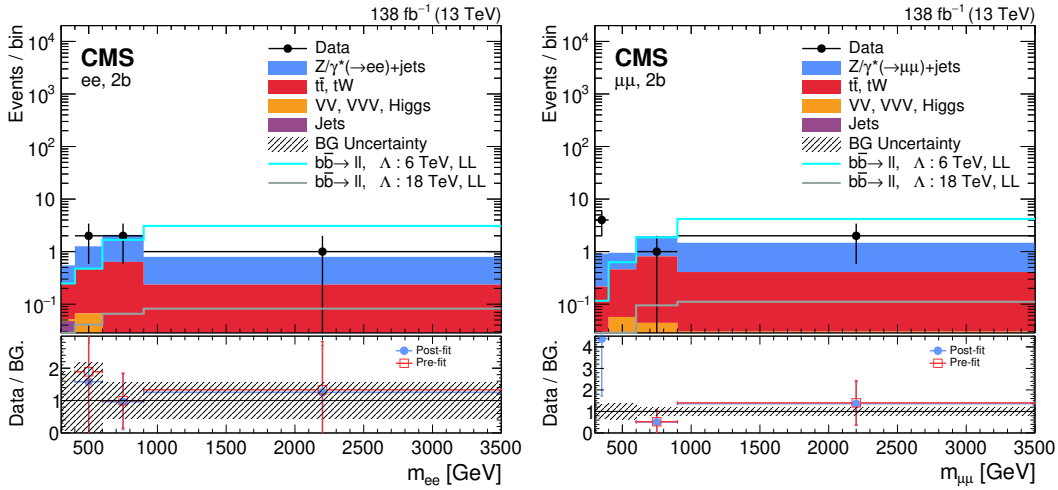

Figure 11. Observed $m_{\ell\ell}$ distributions in the data, and the post-fit backgrounds (stacked histograms), in the SR for ee+2b (left) and $\mu\mu$+2b (right) channels. The lower panels show ratios of the data to the pre-fit background prediction and post-fit background yield as red open squares and blue points, respectively. The hatched band in the lower panels indicates the systematic component of the post-fit uncertainty. The solid lines in the upper panel correspond to the bb$\ell\ell$ signal expectations, for $\Lambda = 6$ and 18 TeV in the LL constructive interference model.

	ee channel		$\mu\mu$ channel	
$m_{\ell\ell}$ [GeV]	Observed yield	Total background	Observed yield	Total background
200–300	108 042	107 890 ± 940	161 236	161 000 ± 440
300–400	26 639	26 640 ± 240	40 982	41 700 ± 120
400–500	9 004	9 093 ± 84	14 135	14 370 ± 53
500–700	5 482	5 536 ± 53	8 530	8 738 ± 39
700–1100	1 885	1 910 ± 21	2 762	2 852 ± 16
1100–1900	323	325.6 ± 4.4	429	457.6 ± 4.7
>1900	29	21.01 ± 0.55	30	33.0 ± 1.4

Table 6. Post-fit event yields for ee and $\mu\mu$ channels in the 0b final state, in the SR. The uncertainties include both statistical and systematic contributions.

compatible with the previous measurement, without a b-tagged jet requirement, performed with the Run 2 data set by the CMS experiment [1], which showed a slight excess of events in the ee channel for masses above 1.8 TeV.

Tables 6–8 show the number of events for various mass ranges for the ee and $\mu\mu$ channels in the 0b, 1b, and 2b final states. The uncertainty in the total background is calculated taking into account correlations in the uncertainties among the different background sources. All values are post-fit and correspond to the SR.

The analysis also tests for lepton flavor universality by measuring the ratio of the differential production cross sections in the $\mu\mu$ and ee channels ($R_{\mu^+\mu^-/e^+e^-}$) as a function of the dilepton invariant mass. The ee and $\mu\mu$ mass distributions are not directly comparable because of the differences in the detector acceptance and lepton efficiencies, as well as the differences in mass scale and resolution between the final states. To address these limitations,

JHEP02(2026)141

	ee channel		$\mu\mu$ channel	
$m_{\ell\ell}$ [GeV]	Observed yield	Total background	Observed yield	Total background
200–300	44	52.8 ± 4.3	127	116 ± 6.3
300–400	35	31.4 ± 2.9	49	47 ± 4.2
400–500	11	16.0 ± 1.7	26	28 ± 2.7
500–700	28	20.2 ± 2.5	39	30 ± 2.9
700–1100	17	11.4 ± 1.2	27	22 ± 2.0
1100–1900	4	2.76 ± 0.41	6	4.65 ± 0.51
>1900	0	0.28 ± 0.11	1	0.58 ± 0.40

Table 7. Post-fit event yields for ee and $\mu\mu$ channels in the 1b final state, in the SR. The uncertainties include both statistical and systematic contributions.

	ee channel		$\mu\mu$ channel	
$m_{\ell\ell}$ [GeV]	Observed yield	Total background	Observed yield	Total background
200–400	2	2.03 ± 0.95	4	2.53 ± 0.68
400–600	2	1.3 ± 1.2	0	0.94 ± 0.31
600–900	2	2.20 ± 0.95	1	1.90 ± 0.27
>900	1	0.81 ± 0.35	2	1.46 ± 0.08

Table 8. Post-fit event yields for ee and $\mu\mu$ channels in the 2b final state, in the SR. The uncertainties include both statistical and systematic contributions.

the measurement is performed by first correcting the bin-by-bin migration effects due to mass scale and resolution in the ee and $\mu\mu$ reconstruction-level mass distributions using the TUnfold package [57] and then correcting the resulting corrected distribution for detector acceptance and lepton efficiency differences.

The bin-by-bin migration effects are corrected from the reconstruction-level distribution to generator level by using a 2-dimensional histogram of reconstructed versus generated mass (response matrix). The response matrices are obtained from the DY+jets MC events passing the full SR selections for each b-tagged multiplicity region, eta category, data-taking year, and lepton flavor. For the lepton flavor ratio study, the 1b and 2b final states are merged, as the event yields in the 2b region are limited and combining the two improves the statistical precision of the measurement. The reconstructed mass distribution in data after subtracting all SM backgrounds except for DY+jets in each channel is corrected by applying the inverted response matrices. Since the off-diagonal elements of the response matrices are typically at the level of 5–10% relative to the diagonal entries, no regularization is necessary. The resulting corrected mass distribution is compared with the generator-level mass spectra for validation and is in good agreement.

To account for the differences in detector acceptance and lepton efficiencies between the electron and muon channels, a normalization factor is derived, assuming no signal is present in the 200–400 GeV mass range, by taking the ratio of the corrected $\mu\mu$ mass distribution to the corrected ee mass distribution in data. Similarly, a normalization factor is derived for the DY+jets simulation using the ratio of $\mu\mu$ and ee events in the corrected simulated

JHEP02(2026)141

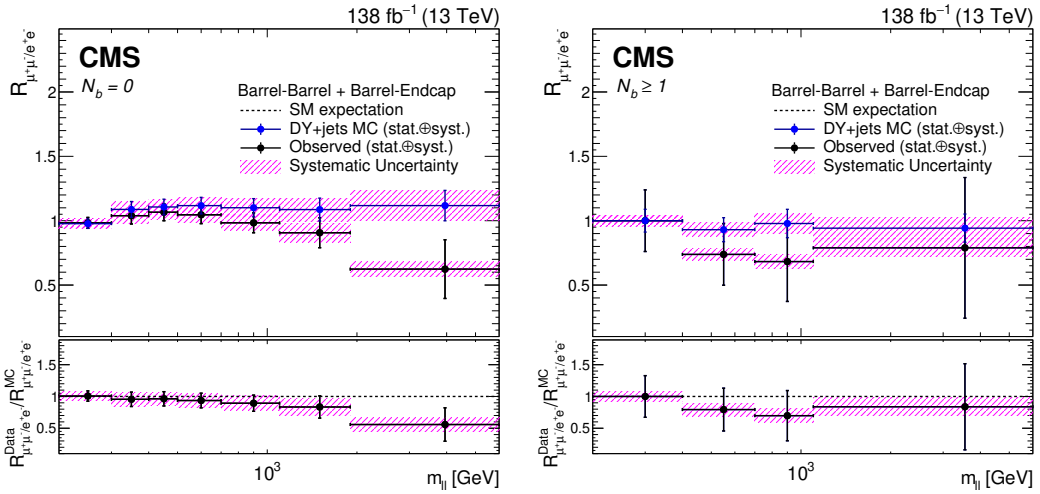

Figure 12. Ratio of the differential dilepton production cross section in the $\mu\mu$ and ee channels as a function of dilepton mass in the 0b (left) and ≥1b (right) final states. The ratio is obtained after correcting the $\mu\mu$ and ee reconstructed mass spectra for bin-by-bin migration effects due to mass scale and resolution. The upper panel shows the observed flavor ratio in data and the DY+jets simulation. The lower panel shows the flavor ratio observed in data and in DY+jets simulation after correcting for the residual differences in acceptance and efficiency as a function of mass. The error bars include both statistical and systematic uncertainties. The shaded band represents the systematic uncertainties in the estimation.

DY+jets mass distribution after full SR selections. Since this normalization is dependent on the jet multiplicity, we derive it for 0b and ≥1b jet final states separately, and independently for each data-taking year and η category. The uncertainty in the factor is taken from the statistical uncertainty of a degree-0 polynomial fit in the 200–400 GeV range and propagated as an additional uncertainty in the ratio. The observed flavor ratio from the corrected mass distributions in data and DY+jets simulation is then corrected with their corresponding normalization factors to obtain the final flavor ratio from data and the DY+jets simulation. As detector acceptance and lepton efficiency differences increase with dilepton invariant mass, the flavor ratio for DY+jets simulation deviates from unity at higher masses as expected.

Most of the systematic uncertainties such as the choice of PDF set, background-specific CR SFs, JES, JER, and b tagging scale factors cancel in the ratio, whereas the remaining systematic uncertainties affecting the mass due to modeling of the mass resolution and scale are propagated to the bin-by-bin migration correction step by obtaining additional response matrices with reconstructed mass values shifted by the uncertainty. The uncertainties in the detector acceptance and lepton efficiencies are propagated to the final flavor ratio via the acceptance and efficiency corrections. In addition, the uncertainties in the normalization factor are also propagated to the final flavor ratio. The dominant systematic contributions across all final states arise from the modeling of the lepton energy scale and resolution, while in the ≥1b jet final state, the limited number of data events provides the largest overall source of uncertainty.

The observed lepton flavor ratio in the 0b final state is shown in figure 12 (left). The upper panel shows the observed flavor ratio in data and in DY+jets simulation. The deviation

JHEP02(2026)141

of the DY+jets simulation flavor ratio from the SM expectation is due to the difference in the acceptance and efficiency of ee and $\mu\mu$ events as a function of mass. The observed flavor ratio is in good agreement with the DY+jets simulation. The small deviation visible at high mass is caused by the slight excess of ee events noted in figure 9, which affects the highest bin of the measured flavor ratio. The lower panel shows the ratio of flavor ratios observed in data and in the DY+jets simulation to correct for the residual differences in acceptance and efficiencies as a function of mass. The observed lepton flavor ratio from corrected ee and $\mu\mu$ mass spectra in the $\geq$1b jet final state can be found in figure 12 (right). Because of limited event counts in the 2b final state, the ratio is estimated by combining the 1b and 2b final states. The observed ratio is consistent with that from the DY+jets simulation. A χ^2 test for the mass range above 400 GeV is performed to quantify the agreement of the observed result with the measurement from the DY+jets simulation. The resulting χ^2/dof value in the 0b final state is 10.86/5, and the one-sided p-value is 0.05. For the $\geq$1b jet final state, the χ^2/dof value is 0.99/3, giving the one-sided p-value as 0.80.

10 Statistical interpretation

Lower limits on the energy scale Λ are obtained by comparing the upper limits on the signal cross section with the prediction calculated with MadGraph5_aMC@NLO at LO. The upper limits on the cross section are computed at 95% confidence level (CL) with Bayesian techniques using the CMS Combine tool [58]. The limits are estimated separately for ee and $\mu\mu$ channels, each time combining all data-taking years and $|\eta|$ categories. The b jet categories are treated differently for the two signals. For the signal cross section a uniform prior is used, whereas the nuisance parameters are modeled with log-normal priors. A binned template based approach is used where the likelihoods are constructed in bins of $m_{\ell\ell}$. For the models with destructive interference, the signal yield is obtained after subtracting the pure LO DY+jets contribution. The interference term becomes dominant for lower mass bins and higher Λ values, therefore the limits are estimated using events above a certain dilepton invariant mass threshold. This mass threshold is optimized to obtain the best expected limits and is found to be 1000 GeV. A combination of the ee and $\mu\mu$ channels is also performed, assuming identical branching fractions into electrons and muons for both signal models.

For the bb$\ell\ell$ signal, the results for the 0b, 1b, and 2b final states are combined in the limit calculation for a particular channel. Figure 13 (upper left) shows the observed lower limits on Λ for the bb$\ell\ell$ signal in the ee final state with constructive and destructive interference and different chirality assumptions. The exclusion for the different chirality and interference assumptions varies within 1 SD. The observed lower limits on Λ for the same model in the $\mu\mu$ channel are shown in figure 13 (upper right). Here, we can see that the exclusions vary within 2 SDs for different chirality and interference assumptions. The difference in observed and expected limits in the ee and $\mu\mu$ channels is due to the slight excess in the 1b final state mass spectra as shown in figure 10. Since the 1b final state is the most sensitive channel, followed by the 0b and 2b channels, this leads to the lower observed limit in both the channels as shown in figure 13. The observed lower limits on Λ for the same model with combined channels are shown in figure 13 (lower plot). The expected and observed lower limits on Λ in the bb$\ell\ell$ signal are summarized in table 9. The limits in the bb$\ell\ell$ signal are stronger than the

JHEP02(2026)141

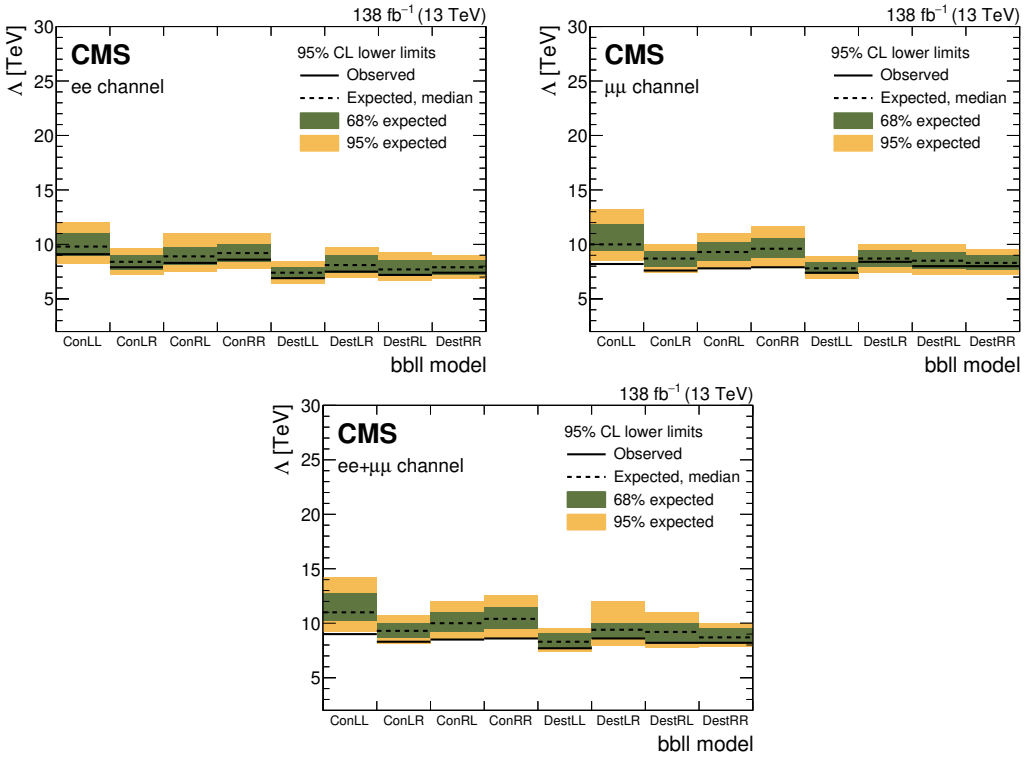

Figure 13. The 95% CL expected and observed lower limits on the energy scale Λ for the bb$\ell\ell$ model with different chirality and interference assumptions, namely constructive left-left (ConLL), left-right (ConLR), right-left (ConRL), right-right (ConRR), destructive left-left (DesLL), left-right (DesLR), right-left (DesRL), and right-right (DesRR) in the ee (upper left), $\mu\mu$ (upper right) channels, and the combination (lower) with $\geq$0 b-tagged jets. The shaded bands correspond to the 68% and 95% quantiles for the expected limits.

		ConLL	ConLR	ConRL	ConRR	DesLL	DesLR	DesRL	DesRR
ee	Expected [TeV]	9.8	8.4	8.9	9.2	7.4	8.1	7.7	7.9
	Observed [TeV]	9.1	7.9	8.3	8.6	6.9	7.5	7.2	7.4
$\mu\mu$	Expected [TeV]	10.0	8.7	9.3	9.6	7.8	8.7	8.5	8.3
	Observed [TeV]	8.2	7.6	7.8	7.9	7.4	8.4	8.0	8.0
Combined	Expected [TeV]	11.0	9.3	10.0	10.4	8.3	9.4	9.2	8.7
	Observed [TeV]	9.0	8.3	8.5	8.6	7.7	8.6	8.2	8.2

Table 9. Lower limits at 95% CL on the energy scale Λ in the bb$\ell\ell$ signal model in TeV for constructive left-left (ConLL), left-right (ConLR), right-left (ConRL), right-right (ConRR), destructive left-left (DesLL), left-right (DesLR), right-left (DesRL), and right-right (DesRR) chirality and interference assumptions in the ee and $\mu\mu$ channels and the combination of the two.

LEP ($e^+e^- \to b\bar{b}$) bounds [59, 60] for the RR/LR/RL chiral structures and both constructive and destructive interference, while for the LL scenario the LEP constraints are tighter.

For the bs$\ell\ell$ signal, the limit is calculated using the 0b and 1b final states. Figure 14 shows the observed limit as a function of Λ/g_* for the ee+0b (left) and $\mu\mu$+0b (right) channels. Figure 15 shows the observed limit as a function of Λ/g_* for the ee+1b (left) and $\mu\mu$+1b

JHEP02(2026)141

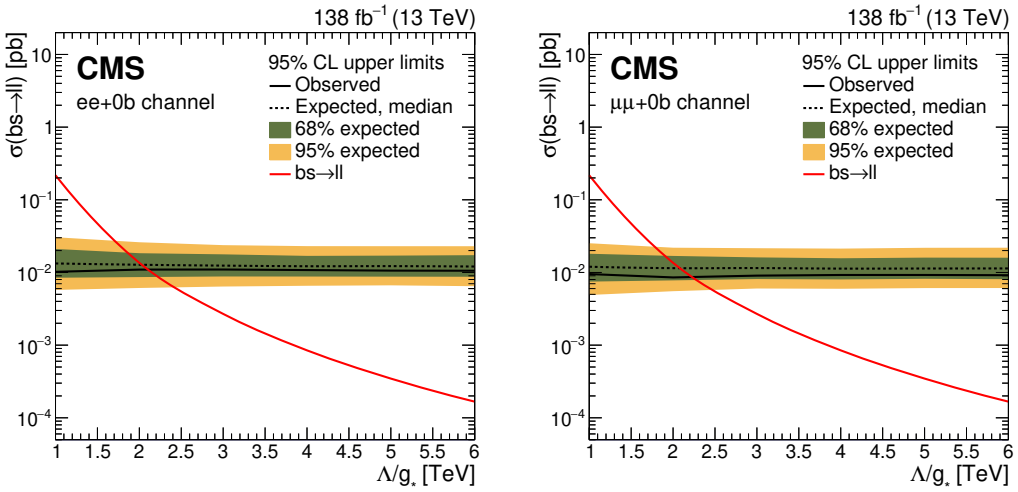

Figure 14. Upper limits at 95% CL on the production cross section for the bs$\ell\ell$ signal in the ee (left) and $\mu\mu$ (right) channels for 0 b-tagged jets. The shaded bands correspond to the 68% and 95% quantiles for the expected limits. The red line corresponds to the theoretical prediction for the bs$\ell\ell$ signal [13].

		0b	1b	combined (0b + 1b)
ee	Expected [TeV]	2.0	2.2	2.3
	Observed [TeV]	2.1	2.0	2.2
$\mu\mu$	Expected [TeV]	2.1	2.3	2.4
	Observed [TeV]	2.2	1.9	2.2
Combined	Expected [TeV]	2.2	2.5	2.6
	Observed [TeV]	2.4	2.0	2.4

Table 10. Lower limits at 95% CL on Λ/g_* in the bs$\ell\ell$ signal model in TeV for 0b, 1b, and combined (0b + 1b) channels. Shown are the expected and observed limits in the ee and $\mu\mu$ channels and the combination of the two.

(right) channels. An observed lower limit on Λ/g_* of 2.1 (2.0) TeV is found for the ee+0b (1b) channel. For the $\mu\mu$+0b (1b) channel, a lower limit of 2.2 (1.9) TeV is observed on Λ/g_*. A 1 (2) SD nonresonant excess in the ee ($\mu\mu$)+1b channel is observed for the bs$\ell\ell$ signal. This slight excess arises because of an increased number of data events, as shown in figure 10, which remain consistent with the predicted background within statistical and systematic uncertainties. The lower limits on Λ/g_* in this model for the 0b, 1b, and combined 0b and 1b channels are summarized in table 10 for the ee, $\mu\mu$, and combined channels. A value of 2.4 TeV is found as the observed lower limit on Λ/g_* for the combination of the two channels. This result is comparable to the existing limits from the LHC experiments [4].

JHEP02(2026)141

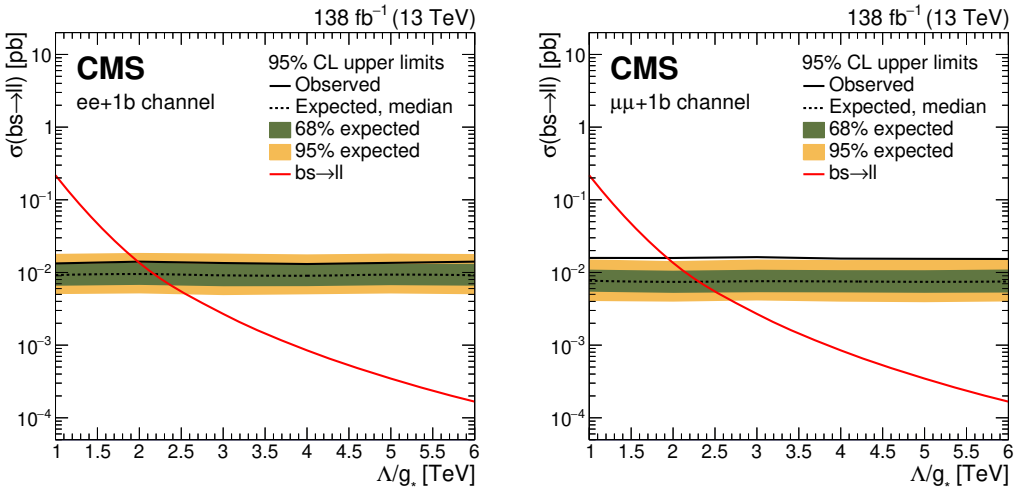

Figure 15. Upper limits at 95% CL on the production cross section for the bs$\ell\ell$ signal in the ee (left) and $\mu\mu$ (right) channels for 1 b-tagged jets. The shaded bands correspond to the 68% and 95% quantiles for the expected limits. The red line corresponds to the theoretical prediction for the bs$\ell\ell$ signal [13].

11 Summary

A search for new physics in the high-mass dilepton final state produced in association with b-tagged jets, focusing on nonresonant phenomena, has been performed using the proton-proton collision data collected during 2016–2018, corresponding to an integrated luminosity of 138 fb^{-1}. Two models of nonresonant signatures have been considered. For a four-fermion contact interaction in bb$\ell\ell$ ($\ell\ell$, electrons or muons) production, lower limits on the scale of new physics (Λ) are set depending on the chirality structure of the interaction and the sign of its interference with the standard model Drell-Yan background. The observed limits are in the range from 6.9 to 9.0 TeV for the bb$\ell\ell$ signal based on different chirality and interference assumptions. These results represent the first LHC constraints on the bb$\ell\ell$ model, significantly extending the sensitivity beyond the limits previously set at LEP. In the bs$\ell\ell$ model, lower limits on the ratio of the energy scale of new physics to the coupling (Λ/g_*) range from 1.9 to 2.2 TeV depending on the channel and 2.4 TeV for the combination of all the channels. Additionally, the ee and $\mu\mu$ invariant mass spectra are compared at the TeV scale. No significant deviation in the lepton flavor ratio from the standard model expectation is observed.

Acknowledgments

We congratulate our colleagues in the CERN accelerator departments for the excellent performance of the LHC and thank the technical and administrative staffs at CERN and at other CMS institutes for their contributions to the success of the CMS effort. In addition, we gratefully acknowledge the computing centers and personnel of the Worldwide LHC Computing Grid and other centers for delivering so effectively the computing infrastructure essential to our analyses. Finally, we acknowledge the enduring support for the construction

JHEP02(2026)141

and operation of the LHC, the CMS detector, and the supporting computing infrastructure provided by the following funding agencies: SC (Armenia), BMBWF and FWF (Austria); FNRS and FWO (Belgium); CNPq, CAPES, FAPERJ, FAPERGS, and FAPESP (Brazil); MES and BNSF (Bulgaria); CERN; CAS, MoST, and NSFC (China); MINCIENCIAS (Colombia); MSES and CSF (Croatia); RIF (Cyprus); SENESCYT (Ecuador); ERC PRG, RVTT3 and MoER TK202 (Estonia); Academy of Finland, MEC, and HIP (Finland); CEA and CNRS/IN2P3 (France); SRNSF (Georgia); BMBF, DFG, and HGF (Germany); GSRI (Greece); NKFIH (Hungary); DAE and DST (India); IPM (Iran); SFI (Ireland); INFN (Italy); MSIP and NRF (Republic of Korea); MES (Latvia); LMTLT (Lithuania); MOE and UM (Malaysia); BUAP, CINVESTAV, CONACYT, LNS, SEP, and UASLP-FAI (Mexico); MOS (Montenegro); MBIE (New Zealand); PAEC (Pakistan); MES and NSC (Poland); FCT (Portugal); MESTD (Serbia); MICIU/AEI and PCTI (Spain); MOSTR (Sri Lanka); Swiss Funding Agencies (Switzerland); MST (Taipei); MHESI and NSTDA (Thailand); TUBITAK and TENMAK (Turkey); NASU (Ukraine); STFC (United Kingdom); DOE and NSF (USA).

Individuals have received support from the Marie-Curie program and the European Research Council and Horizon 2020 Grant, contract Nos. 675440, 724704, 752730, 758316, 765710, 824093, 101115353, 101002207, 101001205, and COST Action CA16108 (European Union); the Leventis Foundation; the Alfred P. Sloan Foundation; the Alexander von Humboldt Foundation; the Science Committee, project no. 22rl-037 (Armenia); the Fonds pour la Formation à la Recherche dans l'Industrie et dans l'Agriculture (FRIA-Belgium); the Beijing Municipal Science & Technology Commission, No. Z191100007219010, the Fundamental Research Funds for the Central Universities, the Ministry of Science and Technology of China under Grant No. 2023YFA1605804, and the Natural Science Foundation of China under Grant No. 12061141002 (China); the Ministry of Education, Youth and Sports (MEYS) of the Czech Republic; the Shota Rustaveli National Science Foundation, grant FR-22-985 (Georgia); the Deutsche Forschungsgemeinschaft (DFG), among others, under Germany's Excellence Strategy — EXC 2121 "Quantum Universe" — 390833306, and under project number 400140256 - GRK2497; the Hellenic Foundation for Research and Innovation (HFRI), Project Number 2288 (Greece); the Hungarian Academy of Sciences, the New National Excellence Program - ÚNKP, the NKFIH research grants K 131991, K 133046, K 138136, K 143460, K 143477, K 146913, K 146914, K 147048, 2020-2.2.1-ED-2021-00181, TKP2021-NKTA-64, and 2021-4.1.2-NEMZ_KI-2024-00036 (Hungary); the Council of Science and Industrial Research, India; ICSC — National Research Center for High Performance Computing, Big Data and Quantum Computing and FAIR — Future Artificial Intelligence Research, funded by the NextGenerationEU program (Italy); the Latvian Council of Science; the Ministry of Education and Science, project no. 2022/WK/14, and the National Science Center, contracts Opus 2021/41/B/ST2/01369 and 2021/43/B/ST2/01552 (Poland); the Fundação para a Ciência e a Tecnologia, grant CEECIND/01334/2018 (Portugal); the National Priorities Research Program by Qatar National Research Fund; MICIU/AEI/10.13039/501100011033, ERDF/EU, "European Union NextGenerationEU/PRTR", and Programa Severo Ochoa del Principado de Asturias (Spain); the Chulalongkorn Academic into Its 2nd Century Project Advancement Project, and the National Science, Research and Innovation Fund via the Program Management Unit for Human Resources & Institutional Development, Research and

Innovation, grant B39G680009 (Thailand); the Kavli Foundation; the Nvidia Corporation; the SuperMicro Corporation; the Welch Foundation, contract C-1845; and the Weston Havens Foundation (USA).

Data Availability Statement. Release and preservation of data used by the CMS Collaboration as the basis for publications is guided by the CMS data preservation, re-use and open access policy, https://doi.org/10.7483/OPENDATA.CMS.1BNU.8V1W.

Code Availability Statement. The CMS core software is publicly available on GitHub https://github.com/cms-sw/cmssw.

References

[1] CMS collaboration, *Search for resonant and nonresonant new phenomena in high-mass dilepton final states at* $\sqrt{s} = 13$ *TeV*, *JHEP* **07** (2021) 208 [arXiv:2103.02708] [INSPIRE].

[2] ATLAS collaboration, *Search for high-mass dilepton resonances using 139* fb^{-1} *of pp collision data collected at* $\sqrt{s} = 13$ *TeV with the ATLAS detector*, *Phys. Lett. B* **796** (2019) 68 [arXiv:1903.06248] [INSPIRE].

[3] ATLAS collaboration, *Search for new non-resonant phenomena in high-mass dilepton final states with the ATLAS detector*, *JHEP* **11** (2020) 005 [*Erratum ibid.* **04** (2021) 142] [arXiv:2006.12946] [INSPIRE].

[4] ATLAS collaboration, *Search for New Phenomena in Final States with Two Leptons and One or No b-Tagged Jets at* $\sqrt{s} = 13$ *TeV Using the ATLAS Detector*, *Phys. Rev. Lett.* **127** (2021) 141801 [arXiv:2105.13847] [INSPIRE].

[5] CMS collaboration, *Search for a high-mass dimuon resonance produced in association with b quark jets at* $\sqrt{s} = 13$ *TeV*, *JHEP* **10** (2023) 043 [arXiv:2307.08708] [INSPIRE].

[6] LHCb collaboration, *Measurement of the ratios of branching fractions* $\mathcal{R}(D^*)$ *and* $\mathcal{R}(D^0)$, *Phys. Rev. Lett.* **131** (2023) 111802 [arXiv:2302.02886] [INSPIRE].

[7] Y. Afik, S. Bar-Shalom, J. Cohen and Y. Rozen, *Searching for New Physics with* $b\bar{b}\ell^+\ell^-$ *contact interactions*, *Phys. Lett. B* **807** (2020) 135541 [arXiv:1912.00425] [INSPIRE].

[8] S. Bar-Shalom, J. Cohen, A. Soni and J. Wudka, *Phenomenology of TeV-scale scalar Leptoquarks in the EFT*, *Phys. Rev. D* **100** (2019) 055020 [arXiv:1812.03178] [INSPIRE].

[9] M. Kramer, T. Plehn, M. Spira and P.M. Zerwas, *Pair production of scalar leptoquarks at the CERN LHC*, *Phys. Rev. D* **71** (2005) 057503 [hep-ph/0411038] [INSPIRE].

[10] I. Dorsner, S. Fajfer and A. Greljo, *Cornering Scalar Leptoquarks at LHC*, *JHEP* **10** (2014) 154 [arXiv:1406.4831] [INSPIRE].

[11] I. Doršner and A. Greljo, *Leptoquark toolbox for precision collider studies*, *JHEP* **05** (2018) 126 [arXiv:1801.07641] [INSPIRE].

[12] S.L. Glashow, J. Iliopoulos and L. Maiani, *Weak Interactions with Lepton-Hadron Symmetry*, *Phys. Rev. D* **2** (1970) 1285 [INSPIRE].

JHEP02(2026)141

[13] Y. Afik et al., *Establishing a Search for $b \to s\ell^+\ell^-$ Anomalies at the LHC*, *JHEP* **08** (2018) 056 [arXiv:1805.11402] [INSPIRE].

[14] S. Patnaik and R. Singh, *A Light Shed on Lepton Flavor Universality in B Decays*, *Universe* **9** (2023) 129 [arXiv:2211.04348] [INSPIRE].

[15] B. Gripaios, M. Nardecchia and S.A. Renner, *Composite leptoquarks and anomalies in B-meson decays*, *JHEP* **05** (2015) 006 [arXiv:1412.1791] [INSPIRE].

[16] A. Greljo and D. Marzocca, *High-p_T dilepton tails and flavor physics*, *Eur. Phys. J. C* **77** (2017) 548 [arXiv:1704.09015] [INSPIRE].

[17] HEPDATA record for this analysis, https://doi.org/10.17182/hepdata.156189.

[18] CMS collaboration, *Performance of the CMS Level-1 trigger in proton-proton collisions at $\sqrt{s} = 13$ TeV*, 2020 *JINST* **15** P10017 [arXiv:2006.10165] [INSPIRE].

[19] CMS collaboration, *The CMS trigger system*, 2017 *JINST* **12** P01020 [arXiv:1609.02366] [INSPIRE].

[20] CMS collaboration, *The CMS Experiment at the CERN LHC*, 2008 *JINST* **3** S08004 [INSPIRE].

[21] D. Contardo et al., *Technical Proposal for the Phase-II Upgrade of the CMS Detector*, CERN-LHCC-2015-010, CMS-TDR-15-02 (2015) [INSPIRE].

[22] G. Busoni et al., *On the Validity of the Effective Field Theory for Dark Matter Searches at the LHC, Part II: Complete Analysis for the s-channel*, *JCAP* **06** (2014) 060 [arXiv:1402.1275] [INSPIRE].

[23] J. Alwall et al., *The automated computation of tree-level and next-to-leading order differential cross sections, and their matching to parton shower simulations*, *JHEP* **07** (2014) 079 [arXiv:1405.0301] [INSPIRE].

[24] R. Frederix and S. Frixione, *Merging meets matching in MC@NLO*, *JHEP* **12** (2012) 061 [arXiv:1209.6215] [INSPIRE].

[25] P. Nason, *A New method for combining NLO QCD with shower Monte Carlo algorithms*, *JHEP* **11** (2004) 040 [hep-ph/0409146] [INSPIRE].

[26] S. Frixione, P. Nason and C. Oleari, *Matching NLO QCD computations with Parton Shower simulations: the POWHEG method*, *JHEP* **11** (2007) 070 [arXiv:0709.2092] [INSPIRE].

[27] S. Alioli, P. Nason, C. Oleari and E. Re, *A general framework for implementing NLO calculations in shower Monte Carlo programs: the POWHEG BOX*, *JHEP* **06** (2010) 043 [arXiv:1002.2581] [INSPIRE].

[28] P. Nason and G. Zanderighi, *W^+W^-, WZ and ZZ production in the POWHEG-BOX-V2*, *Eur. Phys. J. C* **74** (2014) 2702 [arXiv:1311.1365] [INSPIRE].

[29] E. Re, *Single-top Wt-channel production matched with parton showers using the POWHEG method*, *Eur. Phys. J. C* **71** (2011) 1547 [arXiv:1009.2450] [INSPIRE].

[30] S. Alioli, P. Nason, C. Oleari and E. Re, *NLO Higgs boson production via gluon fusion matched with shower in POWHEG*, *JHEP* **04** (2009) 002 [arXiv:0812.0578] [INSPIRE].

[31] P. Nason and C. Oleari, *NLO Higgs boson production via vector-boson fusion matched with shower in POWHEG*, *JHEP* **02** (2010) 037 [arXiv:0911.5299] [INSPIRE].

[32] C. Degrande et al., *UFO — the Universal FeynRules Output*, *Comput. Phys. Commun.* **183** (2012) 1201 [arXiv:1108.2040] [INSPIRE].

JHEP02(2026)141

[33] J. Alwall et al., *Comparative study of various algorithms for the merging of parton showers and matrix elements in hadronic collisions*, *Eur. Phys. J. C* **53** (2008) 473 [arXiv:0706.2569] [INSPIRE].

[34] T. Sjöstrand et al., *An introduction to PYTHIA 8.2*, *Comput. Phys. Commun.* **191** (2015) 159 [arXiv:1410.3012] [INSPIRE].

[35] CMS collaboration, *Extraction and validation of a new set of CMS PYTHIA8 tunes from underlying-event measurements*, *Eur. Phys. J. C* **80** (2020) 4 [arXiv:1903.12179] [INSPIRE].

[36] NNPDF collaboration, *Parton distributions from high-precision collider data*, *Eur. Phys. J. C* **77** (2017) 663 [arXiv:1706.00428] [INSPIRE].

[37] GEANT4 collaboration, *GEANT4 — A Simulation Toolkit*, *Nucl. Instrum. Meth. A* **506** (2003) 250 [INSPIRE].

[38] CMS collaboration, *Pileup mitigation at CMS in 13 TeV data*, 2020 *JINST* **15** P09018 [arXiv:2003.00503] [INSPIRE].

[39] CMS collaboration, *Performance of the CMS electromagnetic calorimeter in pp collisions at* $\sqrt{s} = 13$ *TeV*, 2024 *JINST* **19** P09004 [arXiv:2403.15518] [INSPIRE].

[40] CMS collaboration, *Particle-flow reconstruction and global event description with the CMS detector*, 2017 *JINST* **12** P10003 [arXiv:1706.04965] [INSPIRE].

[41] CMS collaboration, *Electron and photon reconstruction and identification with the CMS experiment at the CERN LHC*, 2021 *JINST* **16** P05014 [arXiv:2012.06888] [INSPIRE].

[42] CMS collaboration, *Performance of the CMS muon trigger system in proton-proton collisions at* $\sqrt{s} = 13$ *TeV*, 2021 *JINST* **16** P07001 [arXiv:2102.04790] [INSPIRE].

[43] CMS collaboration, *Performance of the reconstruction and identification of high-momentum muons in proton-proton collisions at* $\sqrt{s} = 13$ *TeV*, 2020 *JINST* **15** P02027 [arXiv:1912.03516] [INSPIRE].

[44] M. Cacciari, G.P. Salam and G. Soyez, *The anti-*k_t *jet clustering algorithm*, *JHEP* **04** (2008) 063 [arXiv:0802.1189] [INSPIRE].

[45] M. Cacciari, G.P. Salam and G. Soyez, *FastJet User Manual*, *Eur. Phys. J. C* **72** (2012) 1896 [arXiv:1111.6097] [INSPIRE].

[46] E. Bols et al., *Jet Flavour Classification Using DeepJet*, 2020 *JINST* **15** P12012 [arXiv:2008.10519] [INSPIRE].

[47] CMS collaboration, *Performance summary of AK4 jet* b *tagging with data from proton-proton collisions at* $13\,TeV$ *with the CMS detector*, CMS-DP-2023-005.

[48] CMS collaboration, *Identification of heavy-flavour jets with the CMS detector in pp collisions at* 13 *TeV*, 2018 *JINST* **13** P05011 [arXiv:1712.07158] [INSPIRE].

[49] CMS collaboration, *Performance of missing transverse momentum reconstruction in proton-proton collisions at* $\sqrt{s} = 13$ *TeV using the CMS detector*, 2019 *JINST* **14** P07004 [arXiv:1903.06078] [INSPIRE].

[50] CMS collaboration, *Search for high-mass resonances in dilepton final states in proton-proton collisions at* $\sqrt{s} = 13$ *TeV*, *JHEP* **06** (2018) 120 [arXiv:1803.06292] [INSPIRE].

[51] CMS collaboration, *Search for physics beyond the standard model in dilepton mass spectra in proton-proton collisions at* $\sqrt{s} = 8$ *TeV*, *JHEP* **04** (2015) 025 [arXiv:1412.6302] [INSPIRE].

JHEP02(2026)141

[52] CMS collaboration, *Precision luminosity measurement in proton-proton collisions at $\sqrt{s} = 13$ TeV in 2015 and 2016 at CMS*, *Eur. Phys. J. C* **81** (2021) 800 [arXiv:2104.01927] [INSPIRE].

[53] CMS collaboration, *CMS luminosity measurement for the 2017 data-taking period at $\sqrt{s} = 13$ TeV*, CMS-PAS-LUM-17-004 (2018) [INSPIRE].

[54] CMS collaboration, *CMS luminosity measurement for the 2018 data-taking period at $\sqrt{s} = 13$ TeV*, CMS-PAS-LUM-18-002 (2019) [INSPIRE].

[55] CMS collaboration, *Measurement of the inelastic proton-proton cross section at $\sqrt{s} = 13$ TeV*, *JHEP* **07** (2018) 161 [arXiv:1802.02613] [INSPIRE].

[56] J. Butterworth et al., *PDF4LHC recommendations for LHC Run II*, *J. Phys. G* **43** (2016) 023001 [arXiv:1510.03865] [INSPIRE].

[57] S. Schmitt, *TUnfold: an algorithm for correcting migration effects in high energy physics*, 2012 *JINST* **7** T10003 [arXiv:1205.6201] [INSPIRE].

[58] CMS collaboration, *The CMS Statistical Analysis and Combination Tool: Combine*, *Comput. Softw. Big Sci.* **8** (2024) 19 [arXiv:2404.06614] [INSPIRE].

[59] ALEPH et al. collaborations, *A Combination of preliminary electroweak measurements and constraints on the standard model*, hep-ex/0612034 [INSPIRE].

[60] ALEPH et al. collaborations, *Electroweak Measurements in Electron-Positron Collisions at W-Boson-Pair Energies at LEP*, *Phys. Rept.* **532** (2013) 119 [arXiv:1302.3415] [INSPIRE].

JHEP02(2026)141

The CMS collaboration

Yerevan Physics Institute, Yerevan, Armenia

V. Chekhovsky, A. Hayrapetyan, V. Makarenko, A. Tumasyan[1]

Institut für Hochenergiephysik, Vienna, Austria

W. Adam, J.W. Andrejkovic, L. Benato, T. Bergauer, K. Damanakis, M. Dragicevic, C. Giordano, P.S. Hussain, M. Jeitler[2], N. Krammer, A. Li, D. Liko, I. Mikulec, J. Schieck[2], R. Schöfbeck[2], D. Schwarz, M. Sonawane, W. Waltenberger, C.-E. Wulz[2]

Universiteit Antwerpen, Antwerpen, Belgium

T. Janssen, H. Kwon, T. Van Laer, P. Van Mechelen

Vrije Universiteit Brussel, Brussel, Belgium

J. Bierkens, N. Breugelmans, J. D'Hondt, S. Dansana, A. De Moor, M. Delcourt, F. Heyen, Y. Hong, S. Lowette, I. Makarenko, D. Müller, S. Tavernier, M. Tytgat[3], G.P. Van Onsem, S. Van Putte, D. Vannerom

Université Libre de Bruxelles, Bruxelles, Belgium

B. Bilin, B. Clerbaux, A.K. Das, I. De Bruyn, G. De Lentdecker, H. Evard, L. Favart, P. Gianneios, A. Khalilzadeh, F.A. Khan, A. Malara, M.A. Shahzad, L. Thomas, M. Vanden Bemden, C. Vander Velde, P. Vanlaer, F. Zhang

Ghent University, Ghent, Belgium

M. De Coen, D. Dobur, G. Gokbulut, J. Knolle, L. Lambrecht, D. Marckx, K. Skovpen, N. Van Den Bossche, J. van der Linden, J. Vandenbroeck, L. Wezenbeek

Université Catholique de Louvain, Louvain-la-Neuve, Belgium

S. Bein, A. Benecke, A. Bethani, G. Bruno, A. Cappati, J. De Favereau De Jeneret, C. Delaere, A. Giammanco, A.O. Guzel, Sa. Jain, V. Lemaitre, J. Lidrych, P. Mastrapasqua, S. Turkcapar

Centro Brasileiro de Pesquisas Fisicas, Rio de Janeiro, Brazil

G.A. Alves, E. Coelho, G. Correia Silva, C. Hensel, T. Menezes De Oliveira, C. Mora Herrera[4], P. Rebello Teles, M. Soeiro, E.J. Tonelli Manganote[5], A. Vilela Pereira[4]

Universidade do Estado do Rio de Janeiro, Rio de Janeiro, Brazil

W.L. Aldá Júnior, M. Barroso Ferreira Filho, H. Brandao Malbouisson, W. Carvalho, J. Chinellato[6], E.M. Da Costa, G.G. Da Silveira[7], D. De Jesus Damiao, S. Fonseca De Souza, R. Gomes De Souza, S. S. Jesus, T. Laux Kuhn[7], M. Macedo, K. Mota Amarilo, L. Mundim, H. Nogima, J.P. Pinheiro, A. Santoro, A. Sznajder, M. Thiel

Universidade Estadual Paulista, Universidade Federal do ABC, São Paulo, Brazil

C.A. Bernardes[7], L. Calligaris, T.R. Fernandez Perez Tomei, E.M. Gregores, I. Maietto Silverio, P.G. Mercadante, S.F. Novaes, B. Orzari, Sandra S. Padula, V. Scheurer

JHEP02(2026)141

Institute for Nuclear Research and Nuclear Energy, Bulgarian Academy of Sciences, Sofia, Bulgaria
A. Aleksandrov, G. Antchev, R. Hadjiiska, P. Iaydjiev, M. Misheva, M. Shopova, G. Sultanov

University of Sofia, Sofia, Bulgaria
A. Dimitrov, L. Litov, B. Pavlov, P. Petkov, A. Petrov, E. Shumka

Instituto De Alta Investigación, Universidad de Tarapacá, Casilla 7 D, Arica, Chile
S. Keshri, D. Laroze, S. Thakur

Beihang University, Beijing, China
T. Cheng, Q. Guo, T. Javaid, L. Yuan

Department of Physics, Tsinghua University, Beijing, China
Z. Hu, Z. Liang, J. Liu

Institute of High Energy Physics, Beijing, China
G.M. Chen[8], H.S. Chen[8], M. Chen[8], Q. Hou, F. Iemmi, C.H. Jiang, A. Kapoor[9], H. Liao, Z.-A. Liu[10], R. Sharma[11], J.N. Song[10], J. Tao, C. Wang[8], J. Wang, H. Zhang, J. Zhao

State Key Laboratory of Nuclear Physics and Technology, Peking University, Beijing, China
A. Agapitos, Y. Ban, A. Carvalho Antunes De Oliveira, S. Deng, B. Guo, C. Jiang, A. Levin, C. Li, Q. Li, Y. Mao, S. Qian, S.J. Qian, X. Qin, X. Sun, D. Wang, H. Yang, Y. Zhao, C. Zhou

Guangdong Provincial Key Laboratory of Nuclear Science and Guangdong-Hong Kong Joint Laboratory of Quantum Matter, South China Normal University, Guangzhou, China
S. Yang

Sun Yat-Sen University, Guangzhou, China
Z. You

University of Science and Technology of China, Hefei, China
K. Jaffel, N. Lu

Nanjing Normal University, Nanjing, China
G. Bauer[12], B. Li[13], H. Wang, K. Yi[14], J. Zhang

Institute of Modern Physics and Key Laboratory of Nuclear Physics and Ion-beam Application (MOE) - Fudan University, Shanghai, China
Y. Li

JHEP02(2026)141

Zhejiang University, Hangzhou, Zhejiang, China
Z. Lin, C. Lu, M. Xiao

Universidad de Los Andes, Bogota, Colombia
C. Avila, D.A. Barbosa Trujillo, A. Cabrera, C. Florez, J. Fraga, J.A. Reyes Vega

Universidad de Antioquia, Medellin, Colombia
J. Jaramillo, C. Rendón, M. Rodriguez, A.A. Ruales Barbosa, J.D. Ruiz Alvarez

University of Split, Faculty of Electrical Engineering, Mechanical Engineering and Naval Architecture, Split, Croatia
N. Godinovic, D. Lelas, A. Sculac

University of Split, Faculty of Science, Split, Croatia
M. Kovac, A. Petkovic, T. Sculac

Institute Rudjer Boskovic, Zagreb, Croatia
P. Bargassa, V. Brigljevic, B.K. Chitroda, D. Ferencek, K. Jakovcic, A. Starodumov, T. Susa

University of Cyprus, Nicosia, Cyprus
A. Attikis, K. Christoforou, A. Hadjiagapiou, C. Leonidou, J. Mousa, C. Nicolaou, L. Paizanos, F. Ptochos, P.A. Razis, H. Rykaczewski, H. Saka, A. Stepennov

Charles University, Prague, Czech Republic
M. Finger, M. Finger Jr., A. Kveton

Escuela Politecnica Nacional, Quito, Ecuador
E. Ayala

Universidad San Francisco de Quito, Quito, Ecuador
E. Carrera Jarrin

Academy of Scientific Research and Technology of the Arab Republic of Egypt, Egyptian Network of High Energy Physics, Cairo, Egypt
A.A. Abdelalim[15,16], S. Elgammal[17], A. Ellithi Kamel[18]

Center for High Energy Physics (CHEP-FU), Fayoum University, El-Fayoum, Egypt
M. Abdullah Al-Mashad, M.A. Mahmoud

National Institute of Chemical Physics and Biophysics, Tallinn, Estonia
K. Ehataht, M. Kadastik, T. Lange, C. Nielsen, J. Pata, M. Raidal, L. Tani, C. Veelken

Department of Physics, University of Helsinki, Helsinki, Finland
K. Osterberg, M. Voutilainen

JHEP02(2026)141

Helsinki Institute of Physics, Helsinki, Finland
N. Bin Norjoharuddeen, E. Brücken, F. Garcia, P. Inkaew, K.T.S. Kallonen, T. Lampén, K. Lassila-Perini, S. Lehti, T. Lindén, M. Myllymäki, M.m. Rantanen, S. Saariokari, J. Tuominiemi

Lappeenranta-Lahti University of Technology, Lappeenranta, Finland
H. Kirschenmann, P. Luukka, H. Petrow

IRFU, CEA, Université Paris-Saclay, Gif-sur-Yvette, France
M. Besancon, F. Couderc, M. Dejardin, D. Denegri, J.L. Faure, F. Ferri, S. Ganjour, P. Gras, G. Hamel de Monchenault, M. Kumar, V. Lohezic, J. Malcles, F. Orlandi, L. Portales, S. Ronchi, A. Rosowsky, M.Ö. Sahin, A. Savoy-Navarro[19], P. Simkina, M. Titov, M. Tornago

Laboratoire Leprince-Ringuet, CNRS/IN2P3, Ecole Polytechnique, Institut Polytechnique de Paris, Palaiseau, France
F. Beaudette, G. Boldrini, P. Busson, C. Charlot, M. Chiusi, T.D. Cuisset, F. Damas, O. Davignon, A. De Wit, I.T. Ehle, B.A. Fontana Santos Alves, S. Ghosh, A. Gilbert, R. Granier de Cassagnac, L. Kalipoliti, G. Liu, M. Manoni, M. Nguyen, S. Obraztsov, C. Ochando, R. Salerno, J.B. Sauvan, Y. Sirois, G. Sokmen, L. Urda Gómez, E. Vernazza, A. Zabi, A. Zghiche

Université de Strasbourg, CNRS, IPHC UMR 7178, Strasbourg, France
J.-L. Agram[20], J. Andrea, D. Bloch, J.-M. Brom, E.C. Chabert, C. Collard, S. Falke, U. Goerlach, R. Haeberle, A.-C. Le Bihan, M. Meena, O. Poncet, G. Saha, M.A. Sessini, P. Vaucelle

Centre de Calcul de l'Institut National de Physique Nucleaire et de Physique des Particules, CNRS/IN2P3, Villeurbanne, France
A. Di Florio

Institut de Physique des 2 Infinis de Lyon (IP2I), Villeurbanne, France
D. Amram, S. Beauceron, B. Blancon, G. Boudoul, N. Chanon, D. Contardo, P. Depasse, C. Dozen[21], H. El Mamouni, J. Fay, S. Gascon, M. Gouzevitch, C. Greenberg, G. Grenier, B. Ille, E. Jourd'huy, I.B. Laktineh, M. Lethuillier, L. Mirabito, S. Perries, A. Purohit, M. Vander Donckt, P. Verdier, J. Xiao

Georgian Technical University, Tbilisi, Georgia
I. Lomidze, T. Toriashvili[22], Z. Tsamalaidze[23]

RWTH Aachen University, I. Physikalisches Institut, Aachen, Germany
V. Botta, S. Consuegra Rodríguez, L. Feld, K. Klein, M. Lipinski, D. Meuser, V. Oppenländer, A. Pauls, D. Pérez Adán, N. Röwert, M. Teroerde

RWTH Aachen University, III. Physikalisches Institut A, Aachen, Germany
S. Diekmann, A. Dodonova, N. Eich, D. Eliseev, F. Engelke, J. Erdmann, M. Erdmann, B. Fischer, T. Hebbeker, K. Hoepfner, F. Ivone, A. Jung, N. Kumar,

JHEP02(2026)141

M.y. Lee, F. Mausolf, M. Merschmeyer, A. Meyer, F. Nowotny, A. Pozdnyakov, Y. Rath, W. Redjeb, F. Rehm, H. Reithler, V. Sarkisovi, A. Schmidt, C. Seth, A. Sharma, J.L. Spah, F. Torres Da Silva De Araujo[24], S. Wiedenbeck, S. Zaleski

RWTH Aachen University, III. Physikalisches Institut B, Aachen, Germany

C. Dziwok, G. Flügge, T. Kress, A. Nowack, O. Pooth, A. Stahl, T. Ziemons, A. Zotz

Deutsches Elektronen-Synchrotron, Hamburg, Germany

H. Aarup Petersen, M. Aldaya Martin, J. Alimena, S. Amoroso, Y. An, J. Bach, S. Baxter, M. Bayatmakou, H. Becerril Gonzalez, O. Behnke, A. Belvedere, F. Blekman[25], K. Borras[26], A. Campbell, S. Chatterjee, F. Colombina, M. De Silva, G. Eckerlin, D. Eckstein, E. Gallo[25], A. Geiser, V. Guglielmi, M. Guthoff, A. Hinzmann, L. Jeppe, B. Kaech, M. Kasemann, C. Kleinwort, R. Kogler, M. Komm, D. Krücker, W. Lange, D. Leyva Pernia, K. Lipka[27], W. Lohmann[28], F. Lorkowski, R. Mankel, I.-A. Melzer-Pellmann, M. Mendizabal Morentin, A.B. Meyer, G. Milella, K. Moral Figueroa, A. Mussgiller, L.P. Nair, J. Niedziela, A. Nürnberg, J. Park, E. Ranken, A. Raspereza, D. Rastorguev, L. Rygaard, M. Scham[29,26], S. Schnake[26], P. Schütze, C. Schwanenberger[25], D. Selivanova, K. Sharko, M. Shchedrolosiev, D. Stafford, F. Vazzoler, A. Ventura Barroso, R. Walsh, D. Wang, Q. Wang, K. Wichmann, L. Wiens[26], C. Wissing, Y. Yang, S. Zakharov, A. Zimermmane Castro Santos

University of Hamburg, Hamburg, Germany

A. Albrecht, M. Antonello, S. Bollweg, M. Bonanomi, P. Connor, K. El Morabit, Y. Fischer, E. Garutti, A. Grohsjean, J. Haller, D. Hundhausen, H.R. Jabusch, G. Kasieczka, P. Keicher, R. Klanner, W. Korcari, T. Kramer, C.c. Kuo, V. Kutzner, F. Labe, J. Lange, A. Lobanov, C. Matthies, L. Moureaux, M. Mrowietz, A. Nigamova, K. Nikolopoulos, Y. Nissan, A. Paasch, K.J. Pena Rodriguez, T. Quadfasel, B. Raciti, M. Rieger, D. Savoiu, J. Schindler, P. Schleper, M. Schröder, J. Schwandt, M. Sommerhalder, H. Stadie, G. Steinbrück, A. Tews, R. Ward, B. Wiederspan, M. Wolf

Karlsruher Institut fuer Technologie, Karlsruhe, Germany

S. Brommer, E. Butz, Y.M. Chen, T. Chwalek, A. Dierlamm, G.G. Dincer, U. Elicabuk, N. Faltermann, M. Giffels, A. Gottmann, F. Hartmann[30], R. Hofsaess, M. Horzela, U. Husemann, J. Kieseler, M. Klute, O. Lavoryk, J.M. Lawhorn, M. Link, A. Lintuluoto, S. Maier, M. Mormile, Th. Müller, M. Neukum, M. Oh, E. Pfeffer, M. Presilla, G. Quast, K. Rabbertz, B. Regnery, R. Schmieder, N. Shadskiy, I. Shvetsov, H.J. Simonis, L. Sowa, L. Stockmeier, K. Tauqeer, M. Toms, B. Topko, N. Trevisani, T. Voigtländer, R.F. Von Cube, J. Von Den Driesch, M. Wassmer, S. Wieland, F. Wittig, R. Wolf, X. Zuo

Institute of Nuclear and Particle Physics (INPP), NCSR Demokritos, Aghia Paraskevi, Greece

G. Anagnostou, G. Daskalakis, A. Kyriakis, A. Papadopoulos[30], A. Stakia

JHEP02(2026)141

National and Kapodistrian University of Athens, Athens, Greece
G. Melachroinos, Z. Painesis, I. Paraskevas, N. Saoulidou, K. Theofilatos, E. Tziaferi, K. Vellidis, I. Zisopoulos

National Technical University of Athens, Athens, Greece
T. Chatzistavrou, G. Karapostoli, K. Kousouris, E. Siamarkou, G. Tsipolitis

University of Ioánnina, Ioánnina, Greece
I. Bestintzanos, I. Evangelou, C. Foudas, C. Kamtsikis, P. Katsoulis, P. Kokkas, P.G. Kosmoglou Kioseoglou, N. Manthos, I. Papadopoulos, J. Strologas

HUN-REN Wigner Research Centre for Physics, Budapest, Hungary
D. Druzhkin, C. Hajdu, D. Horvath[31,32], K. Márton, A.J. Rádl[33], F. Sikler, V. Veszpremi

MTA-ELTE Lendület CMS Particle and Nuclear Physics Group, Eötvös Loránd University, Budapest, Hungary
M. Csanád, K. Farkas, A. Fehérkuti[34], M.M.A. Gadallah[35], Á. Kadlecsik, G. Pásztor, G.I. Veres

Faculty of Informatics, University of Debrecen, Debrecen, Hungary
B. Ujvari, G. Zilizi

HUN-REN ATOMKI - Institute of Nuclear Research, Debrecen, Hungary
G. Bencze, S. Czellar, J. Molnar, Z. Szillasi

Karoly Robert Campus, MATE Institute of Technology, Gyongyos, Hungary
T. Csorgo[34], F. Nemes[34], T. Novak

Panjab University, Chandigarh, India
S. Bansal, S.B. Beri, V. Bhatnagar, G. Chaudhary, S. Chauhan, N. Dhingra[36], A. Kaur, A. Kaur, H. Kaur, M. Kaur, S. Kumar, T. Sheokand, J.B. Singh, A. Singla

University of Delhi, Delhi, India
A. Bhardwaj, A. Chhetri, B.C. Choudhary, A. Kumar, A. Kumar, M. Naimuddin, K. Ranjan, M.K. Saini, S. Saumya

Indian Institute of Technology Kanpur, Kanpur, India
S. Mukherjee

Saha Institute of Nuclear Physics, HBNI, Kolkata, India
S. Baradia, S. Barman[37], S. Bhattacharya, S. Das Gupta, S. Dutta, S. Dutta, S. Sarkar

Indian Institute of Technology Madras, Madras, India
M.M. Ameen, P.K. Behera, S.C. Behera, S. Chatterjee, G. Dash, A. Dattamunsi, P. Jana, P. Kalbhor, S. Kamble, J.R. Komaragiri[38], D. Kumar[38], T. Mishra,

JHEP02(2026)141

B. Parida[39], P.R. Pujahari, N.R. Saha, A.K. Sikdar, R.K. Singh, P. Verma, S. Verma, A. Vijay

Tata Institute of Fundamental Research-A, Mumbai, India

S. Dugad, G.B. Mohanty, M. Shelake, P. Suryadevara

Tata Institute of Fundamental Research-B, Mumbai, India

A. Bala, S. Banerjee, S. Bhowmik[40], R.M. Chatterjee, M. Guchait, Sh. Jain, A. Jaiswal, B.M. Joshi, S. Kumar, G. Majumder, K. Mazumdar, S. Parolia, A. Thachayath

National Institute of Science Education and Research, An OCC of Homi Bhabha National Institute, Bhubaneswar, Odisha, India

S. Bahinipati[41], D. Maity[42], P. Mal, K. Naskar[42], A. Nayak[42], S. Nayak, K. Pal, R. Raturi, P. Sadangi, S.K. Swain, S. Varghese[42], D. Vats[42]

Indian Institute of Science Education and Research (IISER), Pune, India

S. Acharya[43], A. Alpana, S. Dube, B. Gomber[43], P. Hazarika, B. Kansal, A. Laha, B. Sahu[43], S. Sharma, K.Y. Vaish

Isfahan University of Technology, Isfahan, Iran

H. Bakhshiansohi[44], A. Jafari[45], M. Zeinali[46]

Institute for Research in Fundamental Sciences (IPM), Tehran, Iran

S. Bashiri, S. Chenarani[47], S.M. Etesami, Y. Hosseini, M. Khakzad, E. Khazaie, M. Mohammadi Najafabadi, S. Tizchang[48]

University College Dublin, Dublin, Ireland

M. Felcini, M. Grunewald

INFN Sezione di Bari[a], Università di Bari[b], Politecnico di Bari[c], Bari, Italy

M. Abbrescia[a,b], M. Barbieri[a,b], M. Buonsante[a,b], A. Colaleo[a,b], D. Creanza[a,c], B. D'Anzi[a,b], N. De Filippis[a,c], M. De Palma[a,b], W. Elmetenawee[a,b,15], N. Ferrara[a,b], L. Fiore[a], G. Iaselli[a,c], L. Longo[a], M. Louka[a,b], G. Maggi[a,c], M. Maggi[a], I. Margjeka[a], V. Mastrapasqua[a,b], S. My[a,b], S. Nuzzo[a,b], A. Pellecchia[a,b], A. Pompili[a,b], G. Pugliese[a,c], R. Radogna[a,b], D. Ramos[a], A. Ranieri[a], L. Silvestris[a], F.M. Simone[a,c], Ü. Sözbilir[a], A. Stamerra[a,b], D. Troiano[a,b], R. Venditti[a,b], P. Verwilligen[a], A. Zaza[a,b]

INFN Sezione di Bologna[a], Università di Bologna[b], Bologna, Italy

G. Abbiendi[a], C. Battilana[a,b], D. Bonacorsi[a,b], P. Capiluppi[a,b], A. Castro[†,a,b], F.R. Cavallo[a], M. Cuffiani[a,b], G.M. Dallavalle[a], T. Diotalevi[a,b], F. Fabbri[a], A. Fanfani[a,b], D. Fasanella[a], P. Giacomelli[a], L. Giommi[a,b], C. Grandi[a], L. Guiducci[a,b], S. Lo Meo[a,49], M. Lorusso[a,b], L. Lunerti[a], S. Marcellini[a], G. Masetti[a], F.L. Navarria[a,b], G. Paggi[a,b], A. Perrotta[a], F. Primavera[a,b], A.M. Rossi[a,b], S. Rossi Tisbeni[a,b], T. Rovelli[a,b], G.P. Siroli[a,b]

INFN Sezione di Catania[a], Università di Catania[b], Catania, Italy

S. Costa[a,b,50], A. Di Mattia[a], A. Lapertosa[a], R. Potenza[a,b], A. Tricomi[a,b,50]

JHEP02(2026)141

INFN Sezione di Firenze[a], Università di Firenze[b], Firenze, Italy
J. Altork[a], P. Assiouras[a], G. Barbagli[a], G. Bardelli[a,b], M. Bartolini[a,b], A. Calandri[a], B. Camaiani[a,b], A. Cassese[a], R. Ceccarelli[a], V. Ciulli[a,b], C. Civinini[a], R. D'Alessandro[a,b], L. Damenti[a,b], E. Focardi[a,b], T. Kello[a], G. Latino[a,b], P. Lenzi[a,b], M. Lizzo[a], M. Meschini[a], S. Paoletti[a], A. Papanastassiou[a,b], G. Sguazzoni[a], L. Viliani[a]

INFN Laboratori Nazionali di Frascati, Frascati, Italy
L. Benussi, S. Bianco, S. Meola[51], D. Piccolo

INFN Sezione di Genova[a], Università di Genova[b], Genova, Italy
M. Alves Gallo Pereira[a], F. Ferro[a], E. Robutti[a], S. Tosi[a,b]

INFN Sezione di Milano-Bicocca[a], Università di Milano-Bicocca[b], Milano, Italy
A. Benaglia[a], F. Brivio[a], F. Cetorelli[a,b], F. De Guio[a,b], M.E. Dinardo[a,b], P. Dini[a], S. Gennai[a], R. Gerosa[a,b], A. Ghezzi[a,b], P. Govoni[a,b], L. Guzzi[a], G. Lavizzari[a,b], M.T. Lucchini[a,b], M. Malberti[a], S. Malvezzi[a], A. Massironi[a], D. Menasce[a], L. Moroni[a], M. Paganoni[a,b], S. Palluotto[a,b], D. Pedrini[a], A. Perego[a,b], B.S. Pinolini[a], G. Pizzati[a,b], S. Ragazzi[a,b], T. Tabarelli de Fatis[a,b]

INFN Sezione di Napoli[a], Università di Napoli 'Federico II'[b], Napoli, Italy; Università della Basilicata[c], Potenza, Italy; Scuola Superiore Meridionale (SSM)[d], Napoli, Italy
S. Buontempo[a], A. Cagnotta[a,b], F. Carnevali[a,b], N. Cavallo[a,c], C. Di Fraia[a], F. Fabozzi[a,c], A.O.M. Iorio[a,b], L. Lista[a,b,52], P. Paolucci[a,30], B. Rossi[a]

INFN Sezione di Padova[a], Università di Padova[b], Padova, Italy; Universita degli Studi di Cagliari[c], Cagliari, Italy
R. Ardino[a], P. Azzi[a], N. Bacchetta[a,53], P. Bortignon[a], G. Bortolato[a,b], A.C.M. Bulla[a], R. Carlin[a,b], P. Checchia[a], T. Dorigo[a,54], F. Gasparini[a,b], S. Giorgetti[a], E. Lusiani[a], M. Margoni[a,b], A.T. Meneguzzo[a,b], M. Michelotto[a], F. Montecassiano[a], J. Pazzini[a,b], P. Ronchese[a,b], R. Rossin[a,b], F. Simonetto[a,b], M. Tosi[a,b], A. Triossi[a,b], S. Ventura[a], M. Zanetti[a,b], P. Zotto[a,b], A. Zucchetta[a,b], G. Zumerle[a,b]

INFN Sezione di Pavia[a], Università di Pavia[b], Pavia, Italy
A. Braghieri[a], S. Calzaferri[a], D. Fiorina[a], P. Montagna[a,b], M. Pelliccioni[a], V. Re[a], C. Riccardi[a,b], P. Salvini[a], I. Vai[a,b], P. Vitulo[a,b]

INFN Sezione di Perugia[a], Università di Perugia[b], Perugia, Italy
S. Ajmal[a,b], M.E. Ascioti[a,b], G.M. Bilei[a], C. Carrivale[a,b], D. Ciangottini[a,b], L. Fanò[a,b], V. Mariani[a,b], M. Menichelli[a], F. Moscatelli[a,55], A. Rossi[a,b], A. Santocchia[a,b], D. Spiga[a], T. Tedeschi[a,b]

INFN Sezione di Pisa[a], Università di Pisa[b], Scuola Normale Superiore di Pisa[c], Pisa, Italy; Università di Siena[d], Siena, Italy
C. Aimè[a,b], C.A. Alexe[a,c], P. Asenov[a,b], P. Azzurri[a], G. Bagliesi[a], R. Bhattacharya[a], L. Bianchini[a,b], T. Boccali[a], E. Bossini[a], D. Bruschini[a,c], R. Castaldi[a], F. Cattafesta[a,c],

JHEP02(2026)141

M.A. Ciocci[a,b], M. Cipriani[a,b], V. D'Amante[a,d], R. Dell'Orso[a], S. Donato[a,b], R. Forti[a,b], A. Giassi[a], F. Ligabue[a,c], A.C. Marini[a,b], D. Matos Figueiredo[a], A. Messineo[a,b], S. Mishra[a], V.K. Muraleedharan Nair Bindhu[a,b], M. Musich[a,b], S. Nandan[a], F. Palla[a], M. Riggirello[a,c], A. Rizzi[a,b], G. Rolandi[a,c], S. Roy Chowdhury[a,40], T. Sarkar[a], A. Scribano[a], P. Spagnolo[a], F. Tenchini[a,b], R. Tenchini[a], G. Tonelli[a,b], N. Turini[a,d], F. Vaselli[a,c], A. Venturi[a], P.G. Verdini[a]

INFN Sezione di Roma[a], Sapienza Università di Roma[b], Roma, Italy

P. Akrap[a,b], C. Basile[a,b], F. Cavallari[a], L. Cunqueiro Mendez[a,b], F. De Riggi[a,b], D. Del Re[a,b], E. Di Marco[a,b], M. Diemoz[a], F. Errico[a,b], L. Frosina[a,b], R. Gargiulo[a,b], B. Harikrishnan[a,b], F. Lombardi[a,b], E. Longo[a,b], L. Martikainen[a,b], J. Mijuskovic[a,b], G. Organtini[a,b], N. Palmeri[a,b], F. Pandolfi[a], R. Paramatti[a,b], C. Quaranta[a,b], S. Rahatlou[a,b], C. Rovelli[a], F. Santanastasio[a,b], L. Soffi[a], V. Vladimirov[a,b]

INFN Sezione di Torino[a], Università di Torino[b], Torino, Italy; Università del Piemonte Orientale[c], Novara, Italy

N. Amapane[a,b], R. Arcidiacono[a,c], S. Argiro[a,b], M. Arneodo[a,c], N. Bartosik[a,c], R. Bellan[a,b], C. Biino[a], C. Borca[a,b], N. Cartiglia[a], F. Cossio[a], M. Costa[a,b], R. Covarelli[a,b], N. Demaria[a], L. Finco[a], M. Grippo[a,b], B. Kiani[a,b], F. Legger[a], F. Luongo[a,b], C. Mariotti[a], L. Markovic[a,b], S. Maselli[a], A. Mecca[a,b], L. Menzio[a,b], P. Meridiani[a], E. Migliore[a,b], M. Monteno[a], R. Mulargia[a], M.M. Obertino[a,b], G. Ortona[a], L. Pacher[a,b], N. Pastrone[a], M. Ruspa[a,c], F. Siviero[a,b], V. Sola[a,b], A. Solano[a,b], C. Tarricone[a,b], D. Trocino[a], G. Umoret[a,b], R. White[a,b]

INFN Sezione di Trieste[a], Università di Trieste[b], Trieste, Italy

J. Babbar[a,b], S. Belforte[a], V. Candelise[a,b], M. Casarsa[a], F. Cossutti[a], K. De Leo[a], G. Della Ricca[a,b], R. Delli Gatti[a,b]

Kyungpook National University, Daegu, Korea

S. Dogra, J. Hong, J. Kim, D. Lee, H. Lee, J. Lee, S.W. Lee, C.S. Moon, Y.D. Oh, M.S. Ryu, S. Sekmen, B. Tae, Y.C. Yang

Department of Mathematics and Physics - GWNU, Gangneung, Korea

M.S. Kim

Chonnam National University, Institute for Universe and Elementary Particles, Kwangju, Korea

G. Bak, P. Gwak, H. Kim, D.H. Moon

Hanyang University, Seoul, Korea

E. Asilar, J. Choi[56], D. Kim, T.J. Kim, J.A. Merlin, Y. Ryou

Korea University, Seoul, Korea

S. Choi, S. Han, B. Hong, K. Lee, K.S. Lee, S. Lee, J. Yoo

Kyung Hee University, Department of Physics, Seoul, Korea

J. Goh, S. Yang

JHEP02(2026)141

Sejong University, Seoul, Korea
Y. Kang, H. S. Kim, Y. Kim, S. Lee

Seoul National University, Seoul, Korea
J. Almond, J.H. Bhyun, J. Choi, J. Choi, W. Jun, J. Kim, Y.W. Kim, S. Ko, H. Lee, J. Lee, J. Lee, B.H. Oh, S.B. Oh, H. Seo, U.K. Yang, I. Yoon

University of Seoul, Seoul, Korea
W. Jang, D.Y. Kang, S. Kim, B. Ko, J.S.H. Lee, Y. Lee, I.C. Park, Y. Roh, I.J. Watson

Yonsei University, Department of Physics, Seoul, Korea
G. Cho, S. Ha, K. Hwang, B. Kim, K. Lee, H.D. Yoo

Sungkyunkwan University, Suwon, Korea
M. Choi, M.R. Kim, Y. Lee, I. Yu

College of Engineering and Technology, American University of the Middle East (AUM), Dasman, Kuwait
T. Beyrouthy, Y. Gharbia

Kuwait University - College of Science - Department of Physics, Safat, Kuwait
F. Alazemi

Riga Technical University, Riga, Latvia
K. Dreimanis, A. Gaile, C. Munoz Diaz, D. Osite, G. Pikurs, A. Potrebko, M. Seidel, D. Sidiropoulos Kontos

University of Latvia (LU), Riga, Latvia
N.R. Strautnieks

Vilnius University, Vilnius, Lithuania
M. Ambrozas, A. Juodagalvis, A. Rinkevicius, G. Tamulaitis

National Centre for Particle Physics, Universiti Malaya, Kuala Lumpur, Malaysia
I. Yusuff[57], Z. Zolkapli

Universidad de Sonora (UNISON), Hermosillo, Mexico
J.F. Benitez, A. Castaneda Hernandez, H.A. Encinas Acosta, L.G. Gallegos Maríñez, M. León Coello, J.A. Murillo Quijada, A. Sehrawat, L. Valencia Palomo

Centro de Investigacion y de Estudios Avanzados del IPN, Mexico City, Mexico
G. Ayala, H. Castilla-Valdez, H. Crotte Ledesma, E. De La Cruz-Burelo, I. Heredia-De La Cruz[58], R. Lopez-Fernandez, J. Mejia Guisao, A. Sánchez Hernández

Universidad Iberoamericana, Mexico City, Mexico
C. Oropeza Barrera, D.L. Ramirez Guadarrama, M. Ramírez García

JHEP02(2026)141

Benemerita Universidad Autonoma de Puebla, Puebla, Mexico
I. Bautista, F.E. Neri Huerta, I. Pedraza, H.A. Salazar Ibarguen, C. Uribe Estrada

University of Montenegro, Podgorica, Montenegro
I. Bubanja, N. Raicevic

University of Canterbury, Christchurch, New Zealand
P.H. Butler

National Centre for Physics, Quaid-I-Azam University, Islamabad, Pakistan
A. Ahmad, M.I. Asghar, A. Awais, M.I.M. Awan, H.R. Hoorani, W.A. Khan

AGH University of Krakow, Krakow, Poland
V. Avati, A. Bellora[59], L. Forthomme, L. Grzanka, M. Malawski, K. Piotrzkowski

National Centre for Nuclear Research, Swierk, Poland
H. Bialkowska, M. Bluj, M. Górski, M. Kazana, M. Szleper, P. Zalewski

Institute of Experimental Physics, Faculty of Physics, University of Warsaw, Warsaw, Poland
K. Bunkowski, K. Doroba, A. Kalinowski, M. Konecki, J. Krolikowski, A. Muhammad

Warsaw University of Technology, Warsaw, Poland
P. Fokow, K. Pozniak, W. Zabolotny

Laboratório de Instrumentação e Física Experimental de Partículas, Lisboa, Portugal
M. Araujo, D. Bastos, C. Beirão Da Cruz E Silva, A. Boletti, M. Bozzo, T. Camporesi, G. Da Molin, P. Faccioli, M. Gallinaro, J. Hollar, N. Leonardo, G.B. Marozzo, A. Petrilli, M. Pisano, J. Seixas, J. Varela, J.W. Wulff

Faculty of Physics, University of Belgrade, Belgrade, Serbia
P. Adzic, P. Milenovic

VINCA Institute of Nuclear Sciences, University of Belgrade, Belgrade, Serbia
D. Devetak, M. Dordevic, J. Milosevic, L. Nadderd, V. Rekovic, M. Stojanovic

Centro de Investigaciones Energéticas Medioambientales y Tecnológicas (CIEMAT), Madrid, Spain
J. Alcaraz Maestre, Cristina F. Bedoya, J.A. Brochero Cifuentes, Oliver M. Carretero, M. Cepeda, M. Cerrada, N. Colino, B. De La Cruz, A. Delgado Peris, A. Escalante Del Valle, D. Fernández Del Val, J.P. Fernández Ramos, J. Flix, M.C. Fouz, O. Gonzalez Lopez, S. Goy Lopez, J.M. Hernandez, M.I. Josa, J. Llorente Merino, C. Martin Perez, E. Martin Viscasillas, D. Moran, C. M. Morcillo Perez, Á. Navarro Tobar, C. Perez Dengra, A. Pérez-Calero Yzquierdo, J. Puerta Pelayo, I. Redondo, J. Sastre, J. Vazquez Escobar

JHEP02(2026)141

Universidad Autónoma de Madrid, Madrid, Spain
J.F. de Trocóniz

Universidad de Oviedo, Instituto Universitario de Ciencias y Tecnologías Espaciales de Asturias (ICTEA), Oviedo, Spain
B. Alvarez Gonzalez, A. Cardini, J. Cuevas, J. Del Riego Badas, J. Fernandez Menendez, S. Folgueras, I. Gonzalez Caballero, P. Leguina, E. Palencia Cortezon, J. Prado Pico, V. Rodríguez Bouza, A. Soto Rodríguez, A. Trapote, C. Vico Villalba, P. Vischia

Instituto de Física de Cantabria (IFCA), CSIC-Universidad de Cantabria, Santander, Spain
S. Blanco Fernández, I.J. Cabrillo, A. Calderon, J. Duarte Campderros, M. Fernandez, G. Gomez, C. Lasaosa García, R. Lopez Ruiz, C. Martinez Rivero, P. Martinez Ruiz del Arbol, F. Matorras, P. Matorras Cuevas, E. Navarrete Ramos, J. Piedra Gomez, L. Scodellaro, I. Vila, J.M. Vizan Garcia

University of Colombo, Colombo, Sri Lanka
B. Kailasapathy[60], D.D.C. Wickramarathna

University of Ruhuna, Department of Physics, Matara, Sri Lanka
W.G.D. Dharmaratna[61], K. Liyanage, N. Perera

CERN, European Organization for Nuclear Research, Geneva, Switzerland
D. Abbaneo, C. Amendola, E. Auffray, J. Baechler, D. Barney, A. Bermúdez Martínez, M. Bianco, A.A. Bin Anuar, A. Bocci, L. Borgonovi, C. Botta, A. Bragagnolo, E. Brondolin, C.E. Brown, C. Caillol, G. Cerminara, N. Chernyavskaya, D. d'Enterria, A. Dabrowski, A. David, A. De Roeck, M.M. Defranchis, M. Deile, M. Dobson, W. Funk, S. Giani, D. Gigi, K. Gill, F. Glege, M. Glowacki, A. Gruber, J. Hegeman, J.K. Heikkilä, B. Huber, V. Innocente, T. James, P. Janot, O. Kaluzinska, O. Karacheban[28], G. Karathanasis, S. Laurila, P. Lecoq, E. Leutgeb, C. Lourenço, M. Magherini, L. Malgeri, M. Mannelli, M. Matthewman, A. Mehta, F. Meijers, S. Mersi, E. Meschi, M. Migliorini, V. Milosevic, F. Monti, F. Moortgat, M. Mulders, I. Neutelings, S. Orfanelli, F. Pantaleo, G. Petrucciani, A. Pfeiffer, M. Pierini, M. Pitt, H. Qu, D. Rabady, B. Ribeiro Lopes, F. Riti, M. Rovere, H. Sakulin, R. Salvatico, S. Sanchez Cruz, S. Scarfi, M. Selvaggi, A. Sharma, K. Shchelina, P. Silva, P. Sphicas[62], A.G. Stahl Leiton, A. Steen, S. Summers, D. Treille, P. Tropea, D. Walter, J. Wanczyk[63], J. Wang, S. Wuchterl, P. Zehetner, P. Zejdl, W.D. Zeuner

PSI Center for Neutron and Muon Sciences, Villigen, Switzerland
T. Bevilacqua[64], L. Caminada[64], A. Ebrahimi, W. Erdmann, R. Horisberger, Q. Ingram, H.C. Kaestli, D. Kotlinski, C. Lange, M. Missiroli[64], L. Noehte[64], T. Rohe, A. Samalan

ETH Zurich - Institute for Particle Physics and Astrophysics (IPA), Zurich, Switzerland
T.K. Aarrestad, M. Backhaus, G. Bonomelli, C. Cazzaniga, K. Datta, P. De Bryas Dexmiers D'archiac[63], A. De Cosa, G. Dissertori, M. Dittmar, M. Donegà,

JHEP02(2026)141

F. Eble, M. Galli, K. Gedia, F. Glessgen, C. Grab, N. Härringer, T.G. Harte, W. Lustermann, A.-M. Lyon, M. Malucchi, R.A. Manzoni, M. Marchegiani, L. Marchese, A. Mascellani[63], F. Nessi-Tedaldi, F. Pauss, V. Perovic, S. Pigazzini, B. Ristic, R. Seidita, J. Steggemann[63], A. Tarabini, D. Valsecchi, R. Wallny

Universität Zürich, Zurich, Switzerland

C. Amsler[65], P. Bärtschi, M.F. Canelli, G. Celotto, K. Cormier, M. Huwiler, W. Jin, A. Jofrehei, B. Kilminster, S. Leontsinis, S.P. Liechti, A. Macchiolo, P. Meiring, F. Meng, J. Motta, A. Reimers, P. Robmann, M. Senger, E. Shokr, F. Stäger, R. Tramontano

National Central University, Chung-Li, Taiwan

C. Adloff[66], D. Bhowmik, C.M. Kuo, W. Lin, P.K. Rout, P.C. Tiwari[38]

National Taiwan University (NTU), Taipei, Taiwan

L. Ceard, K.F. Chen, Z.g. Chen, A. De Iorio, W.-S. Hou, T.h. Hsu, Y.w. Kao, S. Karmakar, G. Kole, Y.y. Li, R.-S. Lu, E. Paganis, X.f. Su, J. Thomas-Wilsker, L.s. Tsai, D. Tsionou, H.y. Wu, E. Yazgan

High Energy Physics Research Unit, Department of Physics, Faculty of Science, Chulalongkorn University, Bangkok, Thailand

C. Asawatangtrakuldee, N. Srimanobhas, V. Wachirapusitanand

Tunis El Manar University, Tunis, Tunisia

Y. Maghrbi

Çukurova University, Physics Department, Science and Art Faculty, Adana, Turkey

D. Agyel, F. Boran, F. Dolek, I. Dumanoglu[67], E. Eskut, Y. Guler[68], E. Gurpinar Guler[68], C. Isik, O. Kara, A. Kayis Topaksu, Y. Komurcu, G. Onengut, K. Ozdemir[69], A. Polatoz, B. Tali[70], U.G. Tok, E. Uslan, I.S. Zorbakir

Middle East Technical University, Physics Department, Ankara, Turkey

M. Yalvac[71]

Bogazici University, Istanbul, Turkey

B. Akgun, I.O. Atakisi, E. Gülmez, M. Kaya[72], O. Kaya[73], S. Tekten[74]

Istanbul Technical University, Istanbul, Turkey

A. Cakir, K. Cankocak[67,75], S. Sen[76]

Istanbul University, Istanbul, Turkey

O. Aydilek[77], B. Hacisahinoglu, I. Hos[78], B. Kaynak, S. Ozkorucuklu, O. Potok, H. Sert, C. Simsek, C. Zorbilmez

Yildiz Technical University, Istanbul, Turkey

S. Cerci, B. Isildak[79], D. Sunar Cerci, T. Yetkin

JHEP02(2026)141

Institute for Scintillation Materials of National Academy of Science of Ukraine, Kharkiv, Ukraine

A. Boyaryntsev, B. Grynyov

National Science Centre, Kharkiv Institute of Physics and Technology, Kharkiv, Ukraine

L. Levchuk

University of Bristol, Bristol, United Kingdom

D. Anthony, J.J. Brooke, A. Bundock, F. Bury, E. Clement, D. Cussans, H. Flacher, J. Goldstein, H.F. Heath, M.-L. Holmberg, L. Kreczko, S. Paramesvaran, L. Robertshaw, J. Segal, V.J. Smith

Rutherford Appleton Laboratory, Didcot, United Kingdom

A.H. Ball, K.W. Bell, A. Belyaev[80], C. Brew, R.M. Brown, D.J.A. Cockerill, C. Cooke, A. Elliot, K.V. Ellis, J. Gajownik, K. Harder, S. Harper, J. Linacre, K. Manolopoulos, M. Moallemi, D.M. Newbold, E. Olaiya, D. Petyt, T. Reis, A.R. Sahasransu, G. Salvi, T. Schuh, C.H. Shepherd-Themistocleous, I.R. Tomalin, K.C. Whalen, T. Williams

Imperial College, London, United Kingdom

I. Andreou, R. Bainbridge, P. Bloch, O. Buchmuller, C.A. Carrillo Montoya, D. Colling, J.S. Dancu, I. Das, P. Dauncey, G. Davies, M. Della Negra, S. Fayer, G. Fedi, G. Hall, A. Howard, G. Iles, C.R. Knight, P. Krueper, J. Langford, K.H. Law, J. León Holgado, L. Lyons, A.-M. Magnan, B. Maier, S. Mallios, M. Mieskolainen, J. Nash[81], M. Pesaresi, P.B. Pradeep, B.C. Radburn-Smith, A. Richards, A. Rose, L. Russell, K. Savva, C. Seez, R. Shukla, A. Tapper, K. Uchida, G.P. Uttley, T. Virdee[30], M. Vojinovic, N. Wardle, D. Winterbottom

Brunel University, Uxbridge, United Kingdom

J.E. Cole, A. Khan, P. Kyberd, I.D. Reid

Baylor University, Waco, Texas, USA

S. Abdullin, A. Brinkerhoff, E. Collins, M.R. Darwish, J. Dittmann, K. Hatakeyama, V. Hegde, J. Hiltbrand, B. McMaster, J. Samudio, S. Sawant, C. Sutantawibul, J. Wilson

Catholic University of America, Washington, DC, USA

R. Bartek, A. Dominguez, S. Raj, A.E. Simsek, S.S. Yu

The University of Alabama, Tuscaloosa, Alabama, USA

B. Bam, A. Buchot Perraguin, R. Chudasama, S.I. Cooper, C. Crovella, G. Fidalgo, S.V. Gleyzer, E. Pearson, C.U. Perez, P. Rumerio[82], E. Usai, R. Yi

Boston University, Boston, Massachusetts, USA

G. De Castro, Z. Demiragli, C. Erice, C. Fangmeier, C. Fernandez Madrazo, E. Fontanesi, D. Gastler, F. Golf, S. Jeon, J. O'cain, I. Reed, J. Rohlf, K. Salyer, D. Sperka, D. Spitzbart, I. Suarez, A. Tsatsos, A.G. Zecchinelli

JHEP02(2026)141

Brown University, Providence, Rhode Island, USA
G. Barone, G. Benelli, D. Cutts, S. Ellis, L. Gouskos, M. Hadley, U. Heintz, K.W. Ho, J.M. Hogan[83], T. Kwon, G. Landsberg, K.T. Lau, J. Luo, S. Mondal, T. Russell, S. Sagir[84], X. Shen, M. Stamenkovic, N. Venkatasubramanian

University of California, Davis, Davis, California, USA
S. Abbott, B. Barton, C. Brainerd, R. Breedon, H. Cai, M. Calderon De La Barca Sanchez, M. Chertok, M. Citron, J. Conway, P.T. Cox, R. Erbacher, F. Jensen, O. Kukral, G. Mocellin, M. Mulhearn, S. Ostrom, W. Wei, S. Yoo

University of California, Los Angeles, California, USA
K. Adamidis, M. Bachtis, D. Campos, R. Cousins, A. Datta, G. Flores Avila, J. Hauser, M. Ignatenko, M.A. Iqbal, T. Lam, Y.f. Lo, E. Manca, A. Nunez Del Prado, D. Saltzberg, V. Valuev

University of California, Riverside, Riverside, California, USA
R. Clare, J.W. Gary, G. Hanson

University of California, San Diego, La Jolla, California, USA
A. Aportela, A. Arora, J.G. Branson, S. Cittolin, S. Cooperstein, D. Diaz, J. Duarte, L. Giannini, Y. Gu, J. Guiang, R. Kansal, V. Krutelyov, R. Lee, J. Letts, M. Masciovecchio, F. Mokhtar, S. Mukherjee, M. Pieri, D. Primosch, M. Quinnan, V. Sharma, M. Tadel, E. Vourliotis, F. Würthwein, Y. Xiang, A. Yagil

University of California, Santa Barbara - Department of Physics, Santa Barbara, California, USA
A. Barzdukas, L. Brennan, C. Campagnari, K. Downham, C. Grieco, M.M. Hussain, J. Incandela, J. Kim, A.J. Li, P. Masterson, H. Mei, J. Richman, S.N. Santpur, U. Sarica, R. Schmitz, F. Setti, J. Sheplock, D. Stuart, T.Á. Vámi, X. Yan, D. Zhang

California Institute of Technology, Pasadena, California, USA
A. Albert, S. Bhattacharya, A. Bornheim, O. Cerri, J. Mao, H.B. Newman, G. Reales Gutiérrez, M. Spiropulu, J.R. Vlimant, S. Xie, R.Y. Zhu

Carnegie Mellon University, Pittsburgh, Pennsylvania, USA
J. Alison, S. An, P. Bryant, M. Cremonesi, V. Dutta, T. Ferguson, T.A. Gómez Espinosa, A. Harilal, A. Kallil Tharayil, M. Kanemura, C. Liu, T. Mudholkar, S. Murthy, P. Palit, K. Park, M. Paulini, A. Roberts, A. Sanchez, W. Terrill

University of Colorado Boulder, Boulder, Colorado, USA
J.P. Cumalat, W.T. Ford, A. Hart, A. Hassani, N. Manganelli, J. Pearkes, C. Savard, N. Schonbeck, K. Stenson, K.A. Ulmer, S.R. Wagner, N. Zipper, D. Zuolo

JHEP02(2026)141

Cornell University, Ithaca, New York, USA

J. Alexander, X. Chen, D.J. Cranshaw, J. Dickinson, J. Fan, X. Fan, J. Grassi, S. Hogan, P. Kotamnives, J. Monroy, G. Niendorf, M. Oshiro, J.R. Patterson, M. Reid, A. Ryd, J. Thom, P. Wittich, R. Zou

Fermi National Accelerator Laboratory, Batavia, Illinois, USA

M. Albrow, M. Alyari, O. Amram, G. Apollinari, A. Apresyan, L.A.T. Bauerdick, D. Berry, J. Berryhill, P.C. Bhat, K. Burkett, J.N. Butler, A. Canepa, G.B. Cerati, H.W.K. Cheung, F. Chlebana, C. Cosby, G. Cummings, I. Dutta, V.D. Elvira, J. Freeman, A. Gandrakota, Z. Gecse, L. Gray, D. Green, A. Grummer, S. Grünendahl, D. Guerrero, O. Gutsche, R.M. Harris, T.C. Herwig, J. Hirschauer, B. Jayatilaka, S. Jindariani, M. Johnson, U. Joshi, T. Klijnsma, B. Klima, K.H.M. Kwok, S. Lammel, C. Lee, D. Lincoln, R. Lipton, T. Liu, K. Maeshima, D. Mason, P. McBride, P. Merkel, S. Mrenna, S. Nahn, J. Ngadiuba, D. Noonan, S. Norberg, V. Papadimitriou, N. Pastika, K. Pedro, C. Pena[85], F. Ravera, A. Reinsvold Hall[86], L. Ristori, M. Safdari, E. Sexton-Kennedy, N. Smith, A. Soha, L. Spiegel, S. Stoynev, J. Strait, L. Taylor, S. Tkaczyk, N.V. Tran, L. Uplegger, E.W. Vaandering, C. Wang, I. Zoi

University of Florida, Gainesville, Florida, USA

C. Aruta, P. Avery, D. Bourilkov, P. Chang, V. Cherepanov, R.D. Field, C. Huh, E. Koenig, M. Kolosova, J. Konigsberg, A. Korytov, K. Matchev, N. Menendez, G. Mitselmakher, K. Mohrman, A. Muthirakalayil Madhu, N. Rawal, S. Rosenzweig, V. Sulimov, Y. Takahashi, J. Wang

Florida State University, Tallahassee, Florida, USA

T. Adams, A. Al Kadhim, A. Askew, S. Bower, R. Hashmi, R.S. Kim, S. Kim, T. Kolberg, G. Martinez, H. Prosper, P.R. Prova, M. Wulansatiti, R. Yohay, J. Zhang

Florida Institute of Technology, Melbourne, Florida, USA

B. Alsufyani, S. Butalla, S. Das, T. Elkafrawy[87], M. Hohlmann, M. Lavinsky, E. Yanes

University of Illinois Chicago, Chicago, Illinois, USA

M.R. Adams, A. Baty, C. Bennett, R. Cavanaugh, R. Escobar Franco, O. Evdokimov, C.E. Gerber, H. Gupta, M. Hawksworth, A. Hingrajiya, D.J. Hofman, J.h. Lee, D. S. Lemos, C. Mills, S. Nanda, B. Ozek, T. Phan, D. Pilipovic, R. Pradhan, E. Prifti, P. Roy, T. Roy, S. Rudrabhatla, N. Singh, M.B. Tonjes, N. Varelas, M.A. Wadud, Z. Ye, J. Yoo

The University of Iowa, Iowa City, Iowa, USA

M. Alhusseini, D. Blend, K. Dilsiz[88], L. Emediato, G. Karaman, O.K. Köseyan, J.-P. Merlo, A. Mestvirishvili[89], O. Neogi, H. Ogul[90], Y. Onel, A. Penzo, C. Snyder, E. Tiras[91]

JHEP02(2026)141

Johns Hopkins University, Baltimore, Maryland, USA
B. Blumenfeld, J. Davis, A.V. Gritsan, L. Kang, S. Kyriacou, P. Maksimovic, M. Roguljic, J. Roskes, S. Sekhar, M. Swartz

The University of Kansas, Lawrence, Kansas, USA
A. Abreu, L.F. Alcerro Alcerro, J. Anguiano, S. Arteaga Escatel, P. Baringer, A. Bean, Z. Flowers, D. Grove, J. King, G. Krintiras, M. Lazarovits, C. Le Mahieu, J. Marquez, M. Murray, M. Nickel, S. Popescu[92], C. Rogan, C. Royon, S. Sanders, C. Smith, G. Wilson

Kansas State University, Manhattan, Kansas, USA
B. Allmond, R. Gujju Gurunadha, A. Ivanov, K. Kaadze, Y. Maravin, J. Natoli, D. Roy, G. Sorrentino

University of Maryland, College Park, Maryland, USA
A. Baden, A. Belloni, J. Bistany-riebman, S.C. Eno, N.J. Hadley, S. Jabeen, R.G. Kellogg, T. Koeth, B. Kronheim, S. Lascio, P. Major, A.C. Mignerey, S. Nabili, C. Palmer, C. Papageorgakis, M.M. Paranjpe, E. Popova[93], A. Shevelev, L. Wang, L. Zhang

Massachusetts Institute of Technology, Cambridge, Massachusetts, USA
C. Baldenegro Barrera, J. Bendavid, S. Bright-Thonney, I.A. Cali, P.c. Chou, M. D'Alfonso, J. Eysermans, C. Freer, G. Gomez-Ceballos, M. Goncharov, G. Grosso, P. Harris, D. Hoang, D. Kovalskyi, J. Krupa, L. Lavezzo, Y.-J. Lee, K. Long, C. Mcginn, A. Novak, M.I. Park, C. Paus, C. Reissel, C. Roland, G. Roland, S. Rothman, G.S.F. Stephans, Z. Wang, B. Wyslouch, T. J. Yang

University of Minnesota, Minneapolis, Minnesota, USA
B. Crossman, C. Kapsiak, M. Krohn, D. Mahon, J. Mans, B. Marzocchi, M. Revering, R. Rusack, R. Saradhy, N. Strobbe

University of Nebraska-Lincoln, Lincoln, Nebraska, USA
K. Bloom, D.R. Claes, G. Haza, J. Hossain, C. Joo, I. Kravchenko, A. Rohilla, J.E. Siado, W. Tabb, A. Vagnerini, A. Wightman, F. Yan, D. Yu

State University of New York at Buffalo, Buffalo, New York, USA
H. Bandyopadhyay, L. Hay, H.w. Hsia, I. Iashvili, A. Kalogeropoulos, A. Kharchilava, A. Mandal, M. Morris, D. Nguyen, S. Rappoccio, H. Rejeb Sfar, A. Williams, P. Young

Northeastern University, Boston, Massachusetts, USA
G. Alverson, E. Barberis, J. Bonilla, B. Bylsma, M. Campana, J. Dervan, Y. Haddad, Y. Han, I. Israr, A. Krishna, P. Levchenko, J. Li, M. Lu, R. Mccarthy, D.M. Morse, T. Orimoto, A. Parker, L. Skinnari, C.S. Thoreson, E. Tsai, D. Wood

Northwestern University, Evanston, Illinois, USA
S. Dittmer, K.A. Hahn, D. Li, Y. Liu, M. Mcginnis, Y. Miao, D.G. Monk, M.H. Schmitt, A. Taliercio, M. Velasco

JHEP02(2026)141

University of Notre Dame, Notre Dame, Indiana, USA
G. Agarwal, R. Band, R. Bucci, S. Castells, A. Das, R. Goldouzian, M. Hildreth, K. Hurtado Anampa, T. Ivanov, C. Jessop, A. Karneyeu, K. Lannon, J. Lawrence, N. Loukas, L. Lutton, J. Mariano, N. Marinelli, I. Mcalister, T. McCauley, C. Mcgrady, C. Moore, Y. Musienko[23], H. Nelson, M. Osherson, A. Piccinelli, R. Ruchti, A. Townsend, Y. Wan, M. Wayne, H. Yockey, M. Zarucki, L. Zygala

The Ohio State University, Columbus, Ohio, USA
A. Basnet, M. Carrigan, L.S. Durkin, C. Hill, M. Joyce, M. Nunez Ornelas, K. Wei, D.A. Wenzl, B.L. Winer, B. R. Yates

Princeton University, Princeton, New Jersey, USA
H. Bouchamaoui, K. Coldham, P. Das, G. Dezoort, P. Elmer, P. Fackeldey, A. Frankenthal, B. Greenberg, N. Haubrich, K. Kennedy, G. Kopp, S. Kwan, Y. Lai, D. Lange, A. Loeliger, D. Marlow, I. Ojalvo, J. Olsen, F. Simpson, D. Stickland, C. Tully, L.H. Vage

University of Puerto Rico, Mayaguez, Puerto Rico, USA
S. Malik, R. Sharma

Purdue University, West Lafayette, Indiana, USA
A.S. Bakshi, S. Chandra, R. Chawla, A. Gu, L. Gutay, M. Jones, A.W. Jung, M. Liu, G. Negro, N. Neumeister, G. Paspalaki, S. Piperov, J.F. Schulte, A. K. Virdi, F. Wang, A. Wildridge, W. Xie, Y. Yao, Y. Zhong

Purdue University Northwest, Hammond, Indiana, USA
J. Dolen, N. Parashar, A. Pathak

Rice University, Houston, Texas, USA
D. Acosta, A. Agrawal, T. Carnahan, K.M. Ecklund, P.J. Fernández Manteca, S. Freed, P. Gardner, F.J.M. Geurts, T. Huang, I. Krommydas, W. Li, J. Lin, O. Miguel Colin, B.P. Padley, R. Redjimi, J. Rotter, E. Yigitbasi, Y. Zhang

University of Rochester, Rochester, New York, USA
A. Bodek, P. de Barbaro, R. Demina, J.L. Dulemba, A. Garcia-Bellido, O. Hindrichs, A. Khukhunaishvili, N. Parmar, P. Parygin[93], R. Taus

Rutgers, The State University of New Jersey, Piscataway, New Jersey, USA
B. Chiarito, J.P. Chou, S.V. Clark, D. Gadkari, Y. Gershtein, E. Halkiadakis, M. Heindl, C. Houghton, D. Jaroslawski, S. Konstantinou, I. Laflotte, A. Lath, J. Martins, R. Montalvo, K. Nash, J. Reichert, P. Saha, S. Salur, S. Schnetzer, S. Somalwar, R. Stone, S.A. Thayil, S. Thomas, J. Vora

University of Tennessee, Knoxville, Tennessee, USA
D. Ally, A.G. Delannoy, S. Fiorendi, S. Higginbotham, T. Holmes, A.R. Kanuganti, N. Karunarathna, L. Lee, E. Nibigira, S. Spanier

JHEP02(2026)141

Texas A&M University, College Station, Texas, USA

D. Aebi, M. Ahmad, T. Akhter, K. Androsov, A. Bolshov, O. Bouhali[94], R. Eusebi, J. Gilmore, T. Kamon, H. Kim, S. Luo, R. Mueller, A. Safonov

Texas Tech University, Lubbock, Texas, USA

N. Akchurin, J. Damgov, Y. Feng, N. Gogate, Y. Kazhykarim, K. Lamichhane, S.W. Lee, C. Madrid, A. Mankel, T. Peltola, I. Volobouev

Vanderbilt University, Nashville, Tennessee, USA

E. Appelt, Y. Chen, S. Greene, A. Gurrola, W. Johns, R. Kunnawalkam Elayavalli, A. Melo, D. Rathjens, F. Romeo, P. Sheldon, S. Tuo, J. Velkovska, J. Viinikainen

University of Virginia, Charlottesville, Virginia, USA

B. Cardwell, H. Chung, B. Cox, J. Hakala, R. Hirosky, A. Ledovskoy, C. Mantilla, C. Neu, C. Ramón Álvarez

Wayne State University, Detroit, Michigan, USA

S. Bhattacharya, P.E. Karchin

University of Wisconsin - Madison, Madison, Wisconsin, USA

A. Aravind, S. Banerjee, K. Black, T. Bose, E. Chavez, S. Dasu, P. Everaerts, C. Galloni, H. He, M. Herndon, A. Herve, C.K. Koraka, A. Lanaro, S. Lomte, R. Loveless, A. Mallampalli, A. Mohammadi, S. Mondal, G. Parida, L. Pétré, D. Pinna, A. Savin, V. Shang, V. Sharma, W.H. Smith, D. Teague, H.F. Tsoi, W. Vetens, A. Warden

Authors affiliated with an international laboratory covered by a cooperation agreement with CERN

S. Afanasiev, V. Alexakhin, Yu. Andreev, T. Aushev, D. Budkouski, R. Chistov[95], M. Danilov[95], T. Dimova[95], A. Ershov[95], S. Gninenko, I. Golutvin[†], I. Gorbunov, A. Gribushin[95], V. Karjavine, M. Kirsanov, V. Klyukhin[95], O. Kodolova[96,93], V. Korenkov, A. Kozyrev[95], N. Krasnikov, A. Lanev, A. Malakhov, V. Matveev[95], A. Nikitenko[97,96], V. Palichik, V. Perelygin, S. Petrushanko[95], S. Polikarpov[95], O. Radchenko[95], M. Savina, V. Shalaev, S. Shmatov, S. Shulha, Y. Skovpen[95], V. Smirnov, O. Teryaev, I. Tlisova[95], A. Toropin, N. Voytishin, B.S. Yuldashev[†,98], A. Zarubin, I. Zhizhin

Authors affiliated with an institute formerly covered by a cooperation agreement with CERN

G. Gavrilov, V. Golovtcov, Y. Ivanov, L. Uvarov, A. Vorobyev[†], A. Dermenev, N. Golubev, D. Kirpichnikov, V. Gavrilov, N. Lychkovskaya, V. Popov, A. Zhokin, V. Andreev, M. Azarkin, M. Kirakosyan, A. Terkulov, E. Boos, V. Bunichev, M. Dubinin[85], M. Perfilov, V. Savrin, V. Blinov[95], V. Kachanov, S. Slabospitskii, A. Uzunian, A. Babaev, V. Borshch

[†] *Deceased*

[1] *Also at Yerevan State University, Yerevan, Armenia*

JHEP02(2026)141

[2] Also at TU Wien, Vienna, Austria
[3] Also at Ghent University, Ghent, Belgium
[4] Also at Universidade do Estado do Rio de Janeiro, Rio de Janeiro, Brazil
[5] Also at FACAMP - Faculdades de Campinas, Sao Paulo, Brazil
[6] Also at Universidade Estadual de Campinas, Campinas, Brazil
[7] Also at Federal University of Rio Grande do Sul, Porto Alegre, Brazil
[8] Also at University of Chinese Academy of Sciences, Beijing, China
[9] Also at China Center of Advanced Science and Technology, Beijing, China
[10] Also at University of Chinese Academy of Sciences, Beijing, China
[11] Also at China Spallation Neutron Source, Guangdong, China
[12] Now at Henan Normal University, Xinxiang, China
[13] Also at University of Shanghai for Science and Technology, Shanghai, China
[14] Now at The University of Iowa, Iowa City, Iowa, USA
[15] Also at Helwan University, Cairo, Egypt
[16] Now at Zewail City of Science and Technology, Zewail, Egypt
[17] Now at British University in Egypt, Cairo, Egypt
[18] Now at Cairo University, Cairo, Egypt
[19] Also at Purdue University, West Lafayette, Indiana, USA
[20] Also at Université de Haute Alsace, Mulhouse, France
[21] Also at Istinye University, Istanbul, Turkey
[22] Also at Tbilisi State University, Tbilisi, Georgia
[23] Also at an institute formerly covered by a cooperation agreement with CERN
[24] Also at The University of the State of Amazonas, Manaus, Brazil
[25] Also at University of Hamburg, Hamburg, Germany
[26] Also at RWTH Aachen University, III. Physikalisches Institut A, Aachen, Germany
[27] Also at Bergische University Wuppertal (BUW), Wuppertal, Germany
[28] Also at Brandenburg University of Technology, Cottbus, Germany
[29] Also at Forschungszentrum Jülich, Juelich, Germany
[30] Also at CERN, European Organization for Nuclear Research, Geneva, Switzerland
[31] Also at HUN-REN ATOMKI - Institute of Nuclear Research, Debrecen, Hungary
[32] Now at Universitatea Babes-Bolyai - Facultatea de Fizica, Cluj-Napoca, Romania
[33] Also at MTA-ELTE Lendület CMS Particle and Nuclear Physics Group, Eötvös Loránd University, Budapest, Hungary
[34] Also at HUN-REN Wigner Research Centre for Physics, Budapest, Hungary
[35] Also at Physics Department, Faculty of Science, Assiut University, Assiut, Egypt
[36] Also at Punjab Agricultural University, Ludhiana, India
[37] Also at University of Visva-Bharati, Santiniketan, India
[38] Also at Indian Institute of Science (IISc), Bangalore, India
[39] Also at Amity University Uttar Pradesh, Noida, India
[40] Also at UPES - University of Petroleum and Energy Studies, Dehradun, India
[41] Also at IIT Bhubaneswar, Bhubaneswar, India
[42] Also at Institute of Physics, Bhubaneswar, India
[43] Also at University of Hyderabad, Hyderabad, India
[44] Also at Deutsches Elektronen-Synchrotron, Hamburg, Germany
[45] Also at Isfahan University of Technology, Isfahan, Iran
[46] Also at Sharif University of Technology, Tehran, Iran
[47] Also at Department of Physics, University of Science and Technology of Mazandaran, Behshahr, Iran
[48] Also at Department of Physics, Faculty of Science, Arak University, ARAK, Iran
[49] Also at Italian National Agency for New Technologies, Energy and Sustainable Economic Development, Bologna, Italy
[50] Also at Centro Siciliano di Fisica Nucleare e di Struttura Della Materia, Catania, Italy
[51] Also at Università degli Studi Guglielmo Marconi, Roma, Italy
[52] Also at Scuola Superiore Meridionale, Università di Napoli 'Federico II', Napoli, Italy

JHEP02(2026)141

[53] *Also at Fermi National Accelerator Laboratory, Batavia, Illinois, USA*
[54] *Also at Lulea University of Technology, Lulea, Sweden*
[55] *Also at Consiglio Nazionale delle Ricerche - Istituto Officina dei Materiali, Perugia, Italy*
[56] *Also at Institut de Physique des 2 Infinis de Lyon (IP2I), Villeurbanne, France*
[57] *Also at Department of Applied Physics, Faculty of Science and Technology, Universiti Kebangsaan Malaysia, Bangi, Malaysia*
[58] *Also at Consejo Nacional de Ciencia y Tecnología, Mexico City, Mexico*
[59] *Also at INFN Sezione di Torino, Università di Torino, Torino, Italy; Università del Piemonte Orientale, Novara, Italy*
[60] *Also at Trincomalee Campus, Eastern University, Sri Lanka, Nilaveli, Sri Lanka*
[61] *Also at Saegis Campus, Nugegoda, Sri Lanka*
[62] *Also at National and Kapodistrian University of Athens, Athens, Greece*
[63] *Also at Ecole Polytechnique Fédérale Lausanne, Lausanne, Switzerland*
[64] *Also at Universität Zürich, Zurich, Switzerland*
[65] *Also at Stefan Meyer Institute for Subatomic Physics, Vienna, Austria*
[66] *Also at Laboratoire d'Annecy-le-Vieux de Physique des Particules, IN2P3-CNRS, Annecy-le-Vieux, France*
[67] *Also at Near East University, Research Center of Experimental Health Science, Mersin, Turkey*
[68] *Also at Konya Technical University, Konya, Turkey*
[69] *Also at Izmir Bakircay University, Izmir, Turkey*
[70] *Also at Adiyaman University, Adiyaman, Turkey*
[71] *Also at Bozok Universitetesi Rektörlügü, Yozgat, Turkey*
[72] *Also at Marmara University, Istanbul, Turkey*
[73] *Also at Milli Savunma University, Istanbul, Turkey*
[74] *Also at Kafkas University, Kars, Turkey*
[75] *Now at Istanbul Okan University, Istanbul, Turkey*
[76] *Also at Hacettepe University, Ankara, Turkey*
[77] *Also at Erzincan Binali Yildirim University, Erzincan, Turkey*
[78] *Also at Istanbul University - Cerrahpasa, Faculty of Engineering, Istanbul, Turkey*
[79] *Also at Yildiz Technical University, Istanbul, Turkey*
[80] *Also at School of Physics and Astronomy, University of Southampton, Southampton, United Kingdom*
[81] *Also at Monash University, Faculty of Science, Clayton, Australia*
[82] *Also at Università di Torino, Torino, Italy*
[83] *Also at Bethel University, St. Paul, Minnesota, USA*
[84] *Also at Karamanoğlu Mehmetbey University, Karaman, Turkey*
[85] *Also at California Institute of Technology, Pasadena, California, USA*
[86] *Also at United States Naval Academy, Annapolis, Maryland, USA*
[87] *Also at Ain Shams University, Cairo, Egypt*
[88] *Also at Bingol University, Bingol, Turkey*
[89] *Also at Georgian Technical University, Tbilisi, Georgia*
[90] *Also at Sinop University, Sinop, Turkey*
[91] *Also at Erciyes University, Kayseri, Turkey*
[92] *Also at Horia Hulubei National Institute of Physics and Nuclear Engineering (IFIN-HH), Bucharest, Romania*
[93] *Now at another institute formerly covered by a cooperation agreement with CERN*
[94] *Also at Texas A&M University at Qatar, Doha, Qatar*
[95] *Also at another institute formerly covered by a cooperation agreement with CERN*
[96] *Also at Yerevan Physics Institute, Yerevan, Armenia*
[97] *Also at Imperial College, London, United Kingdom*
[98] *Also at Institute of Nuclear Physics of the Uzbekistan Academy of Sciences, Tashkent, Uzbekistan*

JHEP02(2026)141